Magazine of Concrete Research

Theoretical assessment of progressive collapse capacity of reinforced concrete structures

--Manuscript Draft--

Manuscript Number:	MACR-D-16-00319R2
Full Title:	Theoretical assessment of progressive collapse capacity of reinforced concrete structures
Article Type:	Paper- your paper is on Structures research
Corresponding Author:	Kamal Alogla, M.Sc. Structural engineering University of Salford Manchester, UNITED KINGDOM
Corresponding Author Secondary Information:	
Corresponding Author's Institution:	University of Salford
Corresponding Author's Secondary Institution:	
First Author:	Kamal Alogla, M.Sc. Structural engineering
First Author Secondary Information:	
Order of Authors:	Kamal Alogla, M.Sc. Structural engineering
	Laurence Weekes, Dr.
	Levingshan Augusthus Nelson, Dr.
Order of Authors Secondary Information:	
Abstract:	Progressive collapse behaviour of reinforced concrete structures requires consideration of material and geometric nonlinearity, concrete crushing and rebar fracture. Compressive arch action (CAA) and catenary action (CTA) are the main resisting mechanisms against progressive collapse following a column loss. Hence, many studies have concentrated on the development of CAA and CTA in RC beams, but without considering the effect of bar fracture and the reduction in beam effective depth due to concrete crushing. Taking these additional factors into account, an analytical model to predict the structural behaviour of RC beams under column removal scenario (CRS) is proposed in this paper. The proposed model is evaluated and validated with the available experimental results. The evaluation and validation indicate that the proposed model can provide a reliable assessment of RC beam capacity against progressive collapse.
Funding Information:	

Dear Sir / Madam

I am happy to revise the manuscript of title "Theoretical assessment of progressive collapse capacity of reinforced concrete structures" according to the reviewer comments for publication in the Magazine of Concrete Research Journal.

The editor comments and the authors response as follows:

Please choose 3 keywords from the journal's standard list: http://www.icevirtuallibrary.com/pb-assets/for%20authors/MCRkeywordlistOct2015.xlsx Done, and they added in the main manuscript and through submission process.
Figures 15, 16, and 17 still have a low dpi. Please revise to minimum 600 at a width of 10cm. Done.
All figures are still blurry when zoomed in at 100%. Please ensure figures are clear at this resolution. If not, the figure will be blurry in print. For further image guidance, please see: http://www.icevirtuallibrary.com/pb-assets/for%20authors/figure.pdf Done.
Figures are also provided in colour, the meaning of which will be lost when printed in black and white. Please revise files to Grayscale. Done. All figure has been produced so the meaning of which will not be lost when printing in black and white.

Four additional references were added, two recent articles are from the same journal and two of my recent published articles. All the added references were highlighted with different font colour.

Please address all correspondence concerning this manuscript to me at k.d.alogla@edu.salford.ac.uk

Thank you for your consideration of this manuscript.

Sincerely.

Kamal Alogla

Theoretical assessment of progressive collapse capacity of reinforced concrete structures

Kamal Alogla[1] E-mail: k.d.alogla@edu.salford.ac.uk

Laurence Weekes[1] E-mail: L.Weekes@salford.ac.uk

Levingshan Augusthus-Nelson[1] E-mail: l.augusthusnelson@salford.ac.uk

[1]School of Computer Science and Engineering, University of Salford, Manchester, United Kingdom

Abstract

Progressive collapse behaviour of reinforced concrete structures requires consideration of material and geometric nonlinearity, concrete crushing and rebar fracture. Compressive arch action (CAA) and catenary action (CTA) are the main resisting mechanisms against progressive collapse following a column loss. Hence, many studies have concentrated on the development of CAA and CTA in RC beams, but without considering the effect of bar fracture and the reduction in beam effective depth due to concrete crushing. Taking these additional factors into account, an analytical model to predict the structural behaviour of RC beams under column removal scenario (CRS) is proposed in this paper. The proposed model is evaluated and validated with the available experimental results. The evaluation and validation indicate that the proposed model can provide a reliable assessment of RC beam capacity against progressive collapse.

Keywords: Failure; Fracture; Structural Analysis

Notation

A_s , A'_s Area of tensile and compression reinforcement, respectively.

b Width of a beam.

c_m , c_e	Neutral axis depth at the middle joint interface and at the beam end, respectively.
c_i	Concrete compression zone correspond to δ_i.
C_{cm} , C_{ce}	Concrete compressive force acting at the beam end and the middle joint interface, respectively.
C_{se} , C_{sm}	Steel compressive force acting at the beam end and the middle joint interface, respectively.
d	Effective depth of a beam section.
d_i	Effective depth of a beam section at each step of δ_i.
d_m	Modified effective depth of a beam section.
d'	Distance from the extreme compression fibre of concrete to the centroid of compression reinforcement
f_c'	Concrete compressive cylinder strength
f_y , f_u	Yield strength and ultimate tensile strength of reinforcement
G	Shear modulus of steel
h	Depth of a beam section
K	Stiffness of axial restraints
L	Net span length of a one-bay beam
L_1	Beam length at the fracture of first top or bottom bars.
L_2	Beam length at the total failure.
l_e , l_m	Crack width at the beam end and middle joint interfaces, respectively
l_p	Plastic hinge length.
M_e , M_m	Bending moments acting on the beam end and on the joint interface, respectively
N_e , N_m	Axial force at the end and middle of the beam section, respectively.
P	The applied load.
P_{com} , P_{cat}	Applied load at CAA and catenary action, respectively
T_e , T_m	The steel tensile forces at the beam end and at the joint interface, respectively.
u	The axial movement of the lateral restraints.
V_m	Shear force at a middle joint interface

z	The distance from the point of maximum moment to the point of zero moment.
β	Ratio of the depth of the equivalent rectangular stress block to the neutral axis depth
δ	Beam deflection or displacement of the middle joint
δ_D	The deflection at which the onset of catenary action occurs.
δ_c	The deflection corresponds to the peak load at CAA.
δ_u	The deflection at which the collapse occurs.
δ_{Ft} , δ_{Fb}	The deflections at which top and bottom fracture, respectively.
ΔL	Axial extension of the beam.
ε_{cu}	Ultimate compressive strain of concrete.
ε_s, ε_s'	Strain of tension and compression reinforcement, respectively.
$\varepsilon_{se}, \varepsilon_{sm}$	Strain of tension reinforcement at the beam end and at the middle joint, respectively.
ε_y	Yield strain of steel reinforcement
ε_u	Ultimate tensile strain of steel
θ	Rotation of the beam section.
θ_i	Rotation of the beam section at each value of δ_i.
φ	The angle of the tensile action line at catenary action correspond the second bar fracture.

Introduction

Progressive collapse presents a situation where local failure is followed by the collapse of adjoining members, which in turn causes global collapse, that may eventually result in a great loss of life and injury (GSA, 2003). The design of structures against progressive collapse has not been an integral part of conventional structural design (Kim, 2006).

Since the partial collapse of Ronan Point building in the UK in 1968 which was caused by a gas explosion, much attention to problems associated with progressive collapse has been paid. Efforts have been directed at both code provisions and research work to better understand progressive collapse resisting mechanisms in RC structures.

To mitigate and reduce the probability of progressive collapse, a series of guidelines and design specifications have been published (GSA, 2003, DOD, 2004, ODPM, 2004). In the

current guidelines, the mitigation of progressive collapse is achieved either implicitly by ensuring sufficient integrity and ductility of the structural system or explicitly by providing alternate load paths to redistribute the load after a column loss (Jian and Zheng, 2014).

However, research studies are necessary to provide a better understanding of the resisting mechanisms against progressive collapse. Investigating and quantifying these mechanisms has been conducted experimentally, and analytically through numerical work. Due to the expense of experimental work, a few limited experimental tests are available (Regan, 1975, Sasani et al., 2007, Orton, 2007, Yi et al., 2008, Su et al., 2009, Sadek et al., 2011, Yu and Tan, 2013a, Pour et al., 2015, Ahmadi et al., 2016, Hou et al., 2015, Qian and Li, 2015, Alogla et al., 2016b, Alogla et al., 2016a). Other researchers have examined the structural resistance against progressive collapse using finite element analysis performing non-linear static and dynamic analysis (Bao et al., 2008, Alashker et al., 2011, Kim and Yu, 2012, Yu and Tan, 2013a, Yu and Tan, 2013b).

Although studying the structural behaviour of RC structures numerically is always an option; the assumptions and the approaches made through the modelling and the potential issues due to the limitations of finite element software used need to be checked and verified against available experimental data.

Many researchers have proposed analytical models to predict and assess the capacity of RC structures to resist progressive collapse. Regan (Regan, 1975) derived an equation to evaluate catenary behaviour of RC element under CRS. Park and Gamble (Park and Gamble, 2000) developed a model to predict compressive membrane action in RC slabs. Su et al. (Su et al., 2009) and Merola (Merola, 2009) have modified Park's model to calculate CAA capacity of RC beams. Merola pointed out that Park's model can be used for beams and he modified the model by adopting the EC2 (2004) stress block instead of ACI-318 (1977) which is adopted by Park and Gamble (Park and Gamble, 1980).

Yu and Tan (Yu and Tan, 2014) proposed an analytical model to predict CAA capacity of RC beams under CRS, without considering the effect of bar fracture. Jian and Zheng (Jian and Zheng, 2014) introduced a model to calculate and predict the structural behaviour of RC beams under CRS at both CAA and CTA. In their model, the CAA peak load is calculated according to the classic flexural resistance without considering the effect of the arching action. In addition, no consideration for bar fracture was taken into account when developing the model. Reza and Mohajeri 2016(Abbasnia and Nav, 2015) developed a method to calculate the arching action capacity of RC beams to assess the structural robustness against progressive collapse.

Investigation of the developed models has revealed that these models are not capable of capturing the real behaviour of concrete after attaining its ultimate strain. A reduction in

compression zone depth due to concrete crushing has not been addressed in these models. All previous models and approaches assumed that the ultimate concrete strain remains constant as the deflection increases, which is in fact not the actual state as observed from experimental tests. The experimental tests show that after the specimen attained its ultimate capacity and the crushing of concrete has occurred, the compression zone depth decreases. Therefore, the effective beam depth changes and the lever arm decreases. In addition, the fracture of steel reinforcement was not taken into account when developing the models, despite the fact that the experimental test results showed bar fracture during either CAA or CTA.

Therefore, in this paper, a new approach to predict the structural behaviour of RC beams subjected to CRS is introduced, based on equilibrium and geometry compatibility, and including bar fracture.

Assumptions

In terms of analysis methods, the structural members subjected to column loss can be classified into two systems, rigid-plastic and elastic-plastic systems (Eyre, 1997). Figure 1 shows these systems for a RC sub-assemblage under CRS. Many researchers have assumed a rigid-plastic system for restrained concrete members considering zero elastic deformation along the length of the member. For the elastic-plastic system, the elastic deformation in restrained concrete members is taken into account in the model

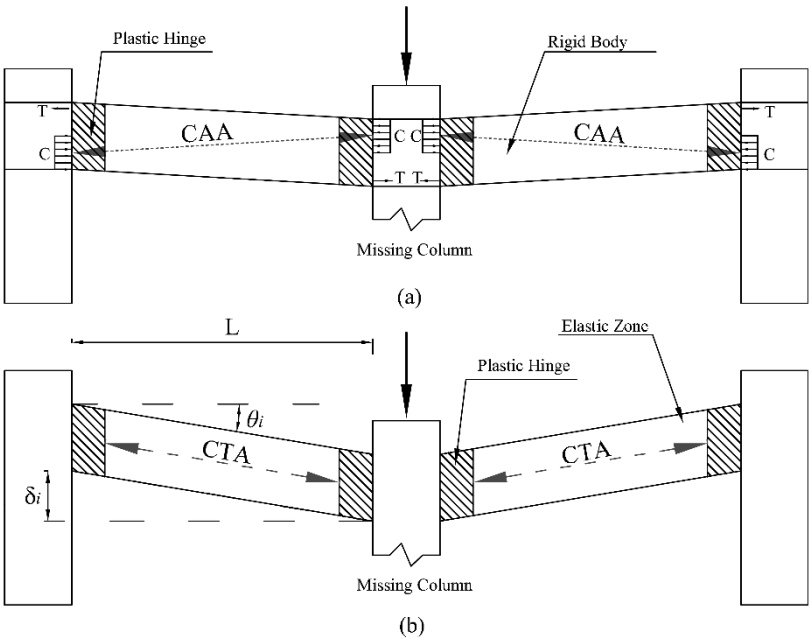

Figure 1: RC sub-assemblage under CRS (a) Rigid-Plastic and (b) Elastic-Plastic.

The rigid-plastic system is considered during the development of the CAA model, while the elastic-plastic system is considered in the development of the CTA model.

In addition to the aforementioned assumptions above, further simplifications are made as follows:

1- For calculation of strains across the section, it is assumed that plane sections before bending remain plane after bending.
2- The bond between steel and concrete is perfect, which dictates that the steel strain is equal to the concrete strain at the same point.
3- Concrete tensile strength is neglected.
4- Crushed concrete is neglected.
5- The stress-strain relationship of the reinforcing steel is assumed to be bilinear. This relationship is valid for both reinforcements in tension and compression, as shown in Figure 2(a).
6- The concrete stress-strain relation as shown in Figure 2(b) with a maximum concrete strain at concrete crushing of 0.0035.

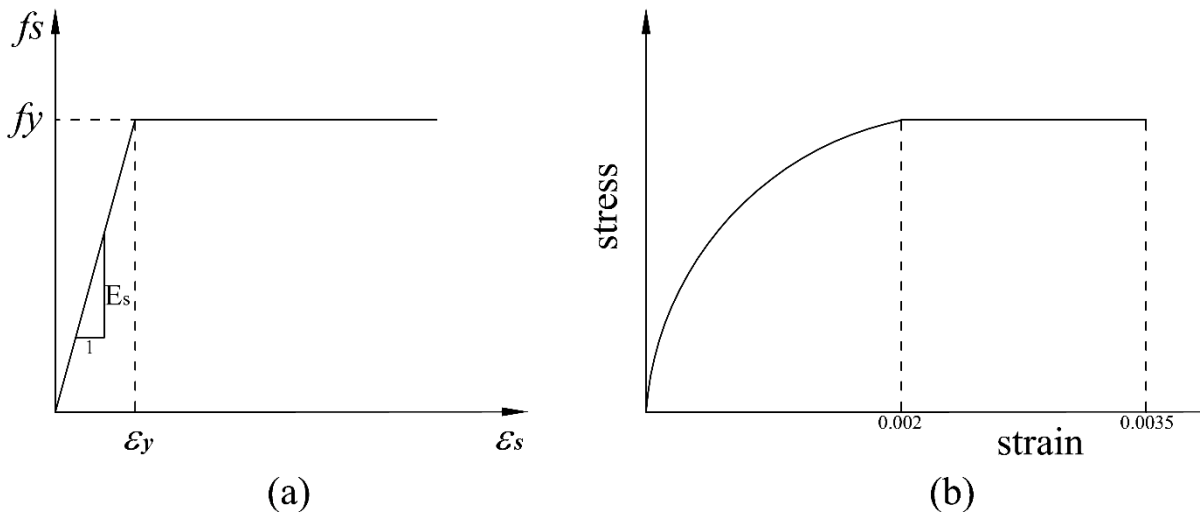

Figure 2: Assumed stress-strain relationship (a) steel and (b) concrete

Procedure for Strain Calculation

The main limitation of the existing models is the assumption of constant ultimate concrete strain ε_{cu} at the extreme fibre after concrete crushing. Crushing of concrete beyond the level of ultimate strain will reduce the effective beam depth (d). Assuming a constant effective depth of beam section for different levels of loading and deflection after concrete crushing can lead to an overestimation of the load capacity of beams under CRS. Figure 3 shows a comparison between the actual strain distribution and the strain distribution based on constant concrete strain in different levels of deflection.

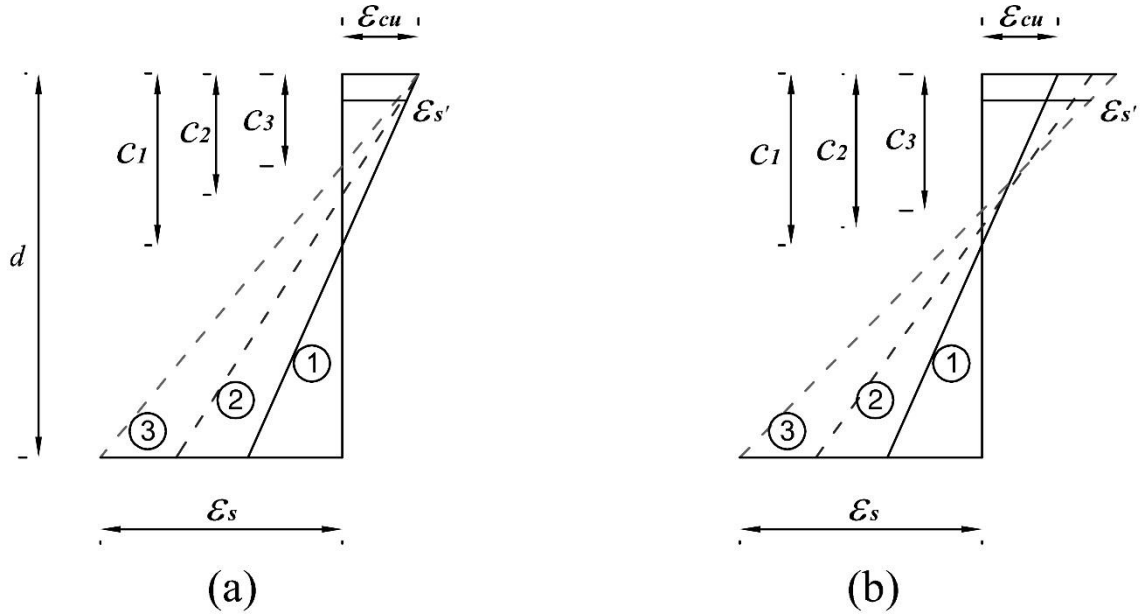

Figure 3: Strain distribution (a) with constant ε_{cu} and (b) actual distribution

As can be seen in figure 3(a), the strain profile progresses from stages 1 to 3, showing that the strain of compression reinforcement (ε_s'), decreases from profile 1 to 3. In fact, the strain of compression reinforcement increases with the increase of deflection until the point where axial compression forces decrease, at which point the strain of these bars start to decrease alerting the onset of catenary action as can be seen in figure 3(b).

In figure 3, c_1 represents the actual compression depth in the beam section corresponding to δ_1, while c_2 and c_3 represent compression depth corresponding to δ_2 and δ_3 respectively, where crushing of concrete is not considered. Compression depths for profiles 2 and 3 require modification because their values include a thickness of crushed concrete. This thickness should be neglected and subtracted from the compression zone depth. Consequently, the beam effective depth should be reduced by the depth of the crushed concrete.

The proposed approach to calculate concrete and steel strains for each value of deflection after concrete crushing is based on dividing the concrete compression zone into small layers as shown in figure 4. When the strain of the top layer exceeds the ultimate concrete strain, the layer is neglected and the effective depth of the beam section is modified according to the triangular geometry and compatibly conditions.

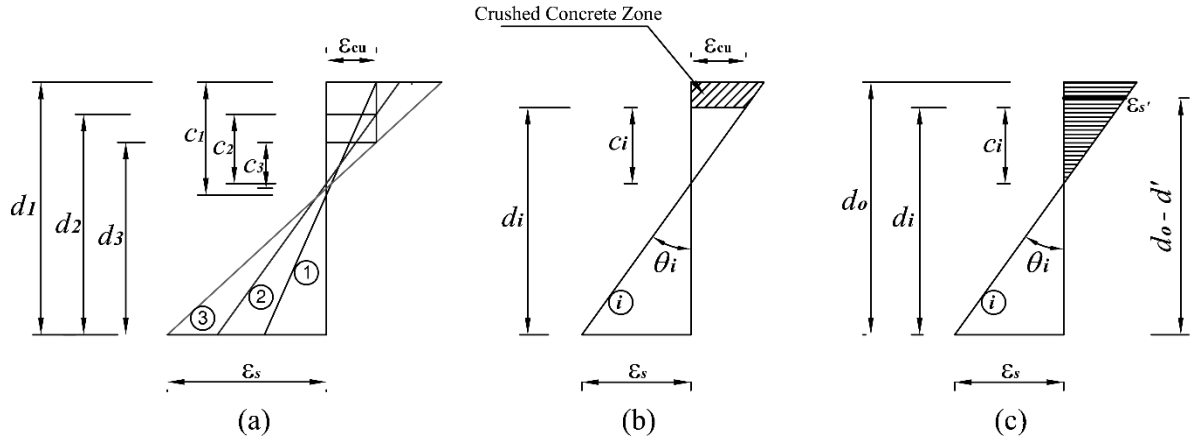

Figure 4: Proposed strain distribution profiles at different deflection values

In order to obtain the thickness of the crushed concrete, a relationship between the deflection and the effective depth is derived. In addition, the strain of compression steel should be calculated dependent on the strain in the tension steel.

From Figure 4(b), the relationship between the effective depth and the concrete compression zone can be derived as follows:

$$\frac{\varepsilon_{cu}}{c_i} = \frac{\varepsilon_s}{d_i - c_i} \tag{1}$$

According to Matthew (2008)(Haskett et al., 2009), the length of strain penetration over the extreme compression fibre is equal to d, therefore:

$$tan(\theta_i) = \frac{\varepsilon_{cu}}{c_i} d_i \tag{2}$$

From Figure 1, the relationship between deflection and beam rotation angle can be obtained as follows:

$$\tan(\theta_i) = \frac{\delta_i}{L} \tag{3}$$

From equation 2 and 3, c_i, c_{i+1} can be obtained as follows:

$$c_i = \frac{L\,\varepsilon_{cu} d_i}{\delta_i} \quad , \quad c_{i+1} = \frac{L\,\varepsilon_{cu} d_{i+1}}{\delta_{i+1}} \tag{4}$$

For each value of δ, there is a layer of concrete that should be neglected and the effective beam depth is therefore modified. To simplify the calculation of the crushed concrete thickness, the depth of the neutral axis is assumed to be constant. Therefore, the crushed concrete thickness (t_i) will be equal to only ($c_i - c_{i+1}$), and can be obtained from equation (5):

$$t_i = \frac{L\,\varepsilon_{cu} d_i}{\delta_i} \times \frac{\delta_{i+1} - \delta_i}{\delta_{i+1} - L\,\varepsilon_{cu}} \tag{5}$$

Therefore, the value of modified effective depth for each deflection or deflection increment can be calculated from equation 6:

$$d_{i+1\,modified} = d_i - t_i \tag{6}$$

From figure 4(c), and from triangular relations, the strains in the tension and compression steel reinforcement can be calculated as follows:

$$\varepsilon_s = \frac{d_i - c_i}{c_i}\varepsilon_{cu}\,, \quad \varepsilon_s' = \frac{d_o - d'}{c_i}\varepsilon_{cu} - \varepsilon_s \tag{7}$$

Development of CAA Model

Figure 6 shows a typical load-deflection relationship of a RC slab strip or a beam subjected to CRS (Park and Gamble, 1980). The relationship can be divided into three sections according to the resisting mechanisms, from A to B flexural action, from B to D compressive arch action and from D to E catenary action. From A to B, the behaviour of beam is elastic, followed by yielding at point B. Due to the effects of CAA, the load increases from B until ultimate capacity at C. From C to D, a reduction in the capacity occurs due to concrete crushing and formation of plastic hinges at critical sections. At point D, which is the onset of CTA, a transition from compressive force into tensile force occurs and the axial force therefore is zero. From D to E, the load capacity increases due to CTA stage. In this section, an analytical model is developed to predict the behaviour of RC beams for the region C to D.

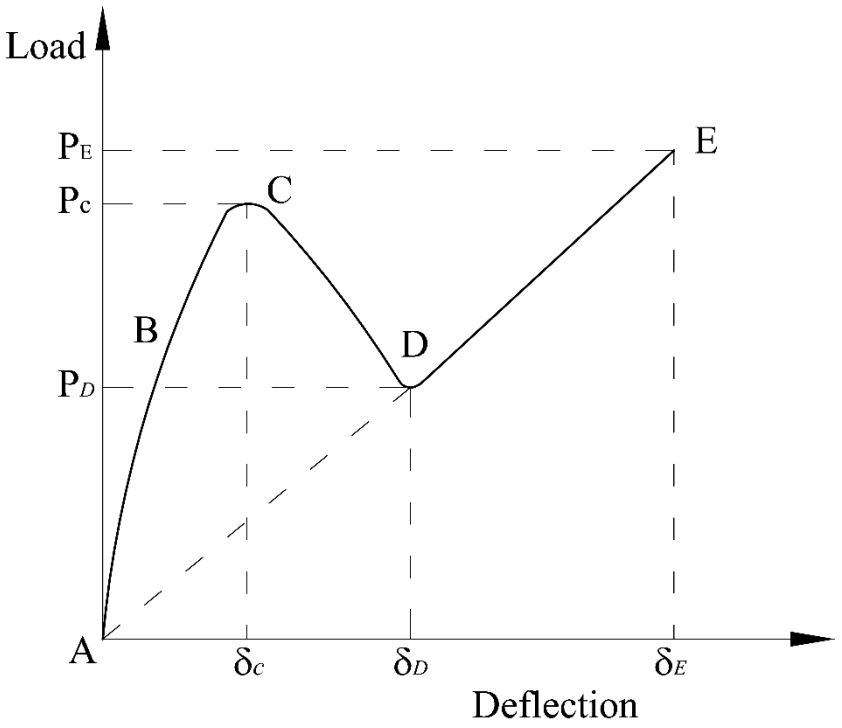

Figure 5: Load-deflection relation of RC slab strip and beam.

Figure 1(a) shows a RC beam sub-assemblage under CAA, and a free body diagram of a single beam and the middle joint subjected to a load P is shown in Figure 6.

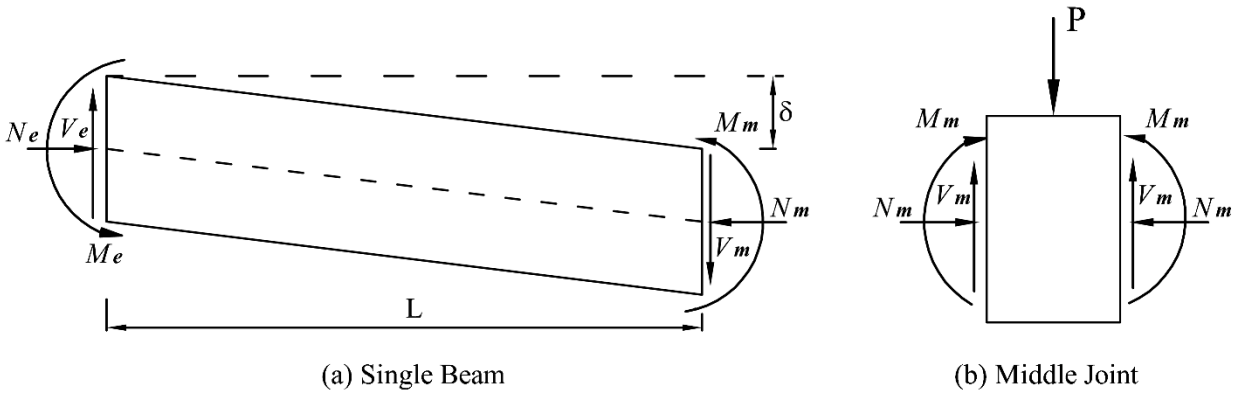

Figure 6: Free Body Diagram of RC Sub-Assemblage (a) single beam and (b) middle joint.

From Figure 6 based on equilibrium, the vertical applied load capacity can be determined as follows:

$$Axial\ Force, \quad N = N_e = N_m \tag{8}$$

$$Shear\ Force, \quad V = V_e = V_m \tag{9}$$

$$Applied\ Load, \quad P = 2V \tag{10}$$

By taking moment equilibrium about the end support in Figure 6(a):

$$V_m L = M_e + M_m - N_m \delta \tag{11}$$

By substituting equations 8, 9 and 10 into equation 11, the load capacity can be obtained:

$$P = \frac{2(M_e + M_m - N\,\delta)}{L} \tag{12}$$

M_e , M_m and N can be calculated based on the internal beam section forces, Figure 7.

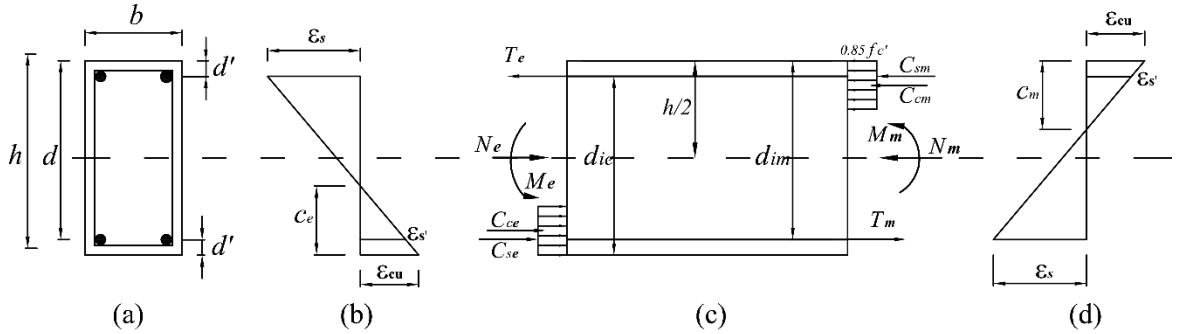

Figure 7: Strain and force distribution (a) beam section, (b) strains at beam end section, (c) moments and forces at beam section and (d) strains at middle joint section.

From moment equilibrium at the beam section and by taking moments about the centre of the beam section, moments M_e and M_m can be obtained as follows:

$$M_e = C_{ce}\left\{\ d_i + d' - \frac{h}{2} - \frac{\beta c_e}{2}\right\} + C_{se}\left\{\frac{h}{2} - \ d'\right\} + T_e\left\{\frac{h}{2} - d'\right\} \tag{13}$$

$$M_m = C_{cm}\left\{\ d_i + d' - \frac{h}{2} - \frac{\beta c_m}{2}\right\} + C_{sm}\left\{\frac{h}{2} - \ d'\right\} + T_m\left\{\frac{h}{2} - \mathrm{d}'\right\} \tag{14}$$

From the equilibrium of horizontal forces, axial forces N_e and N_m can be obtained as follows:

$$N_e = C_{ce} + C_{se} - T_e \tag{15}$$

$$N_m = C_{cm} + C_{sm} - T_m \tag{16}$$

Where C_c , C_s and T are the concrete compressive force, steel compressive force and steel tensile force respectively. The subscripts e and m refer to the beam end and middle joint respectively.

From Figure 7(c), C_c , C_s and T can be calculated as follows:

$$C_c = 0.85 f_c' b \beta c \quad (17)$$

$$C_s = \varepsilon_s' E_s A_s' \quad (18)$$

$$T = f_y A_s \quad (19)$$

Where:

β, is the ratio of the depth of the equivalent stress block to the neutral axis depth.

By substituting equations (15) to (19) into equation (8), the equation of equilibrium will be as follows:

$$0.85 f_c' b \beta c_e + \varepsilon_{se} E_s A_{se}' - f_y A_{se} = 0.85 f_c' b \beta c_m + \varepsilon_{sm}' E_s A_{sm}' - f_y A_{sm} \quad (20)$$

Equation (20) indicates that c_e and c_m are functions of each other. In order to find the values of these unknowns, another equation that can relate c_e with c_m is required. The other equation will be based on compatibility conditions, which can correlate both unknowns c_e and c_m and relate them to the vertical deflection of the middle joint (δ).

Figure 8 shows a single bay beam subjected to a concentrated load at the middle joint, the developed axial compression forces throughout the length of the beam will induce a lateral support movement of a value u. The value of u depends on the support stiffness and the amount of axial compression forces developed under CRS. According to the assumptions, no axial deformation will occur and no support rotation. Therefore, the total horizontal length of the bay beam after joint lateral movement will be equal to ($L + u$).

At the beam end, a crack of width equal to $(h - c_e)\, tan(\theta)$ occurs, and a strain elongation l_e occurs at the tension steel at the top. At the middle joint of the beam, the length of the crushed concrete will be equal to $c_m \tan(\theta)$, and a strain elongation l_m occurs in the tension steel at the bottom.

Therefore, the total length of the bay beam will be equal to $(L + (h - c_e)\, tan(\theta) - c_m\, tan(\theta))$. From triangular geometry relations, the relationship between c_e and c_m can be derived as follows:

$$\delta^2 + (L+u)^2 = (L - c_m \tan(\theta) + (h - c_e)\tan(\theta))^2 \quad (21)$$

$$u = \frac{N}{K} \quad (22)$$

$$\tan(\theta) = \frac{\delta}{L+u} \quad (23)$$

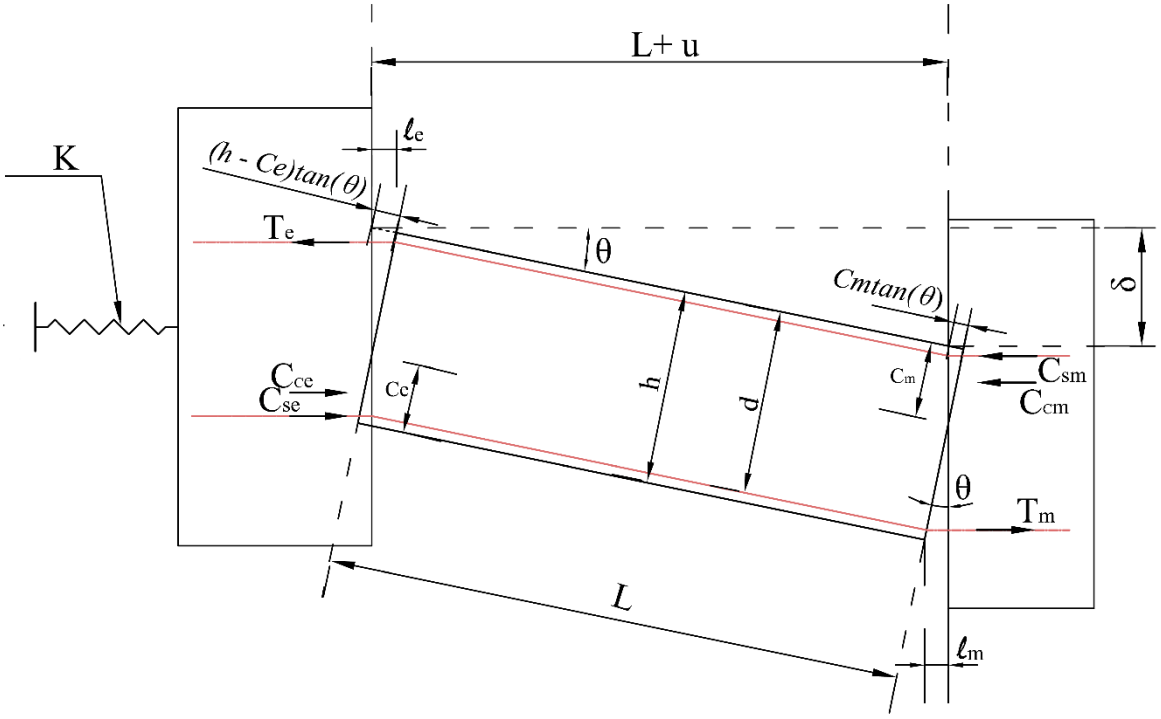

Figure 8: Deflected shape of single bay beam with all internal forces and deformations.

By substituting equations (22) and (23) into equation (21) and rearranging the variables, the relation between c_e and c_m can be expressed in equation 24:

$$c_e + c_m = h - \frac{\delta}{2} - \frac{N}{K}\left(\frac{2L^2 + \delta^2}{2L\delta}\right) \quad (24)$$

Examination of equation (24) indicates that the presence of axial forces in restrained RC beams will increase the compression depth zones. When $N = 0$ in simply supported RC beams, the value of $(c_e + c_m)$ will be equal to $h - \delta/2$ only.

The compatibility equation (24) indicates that for a given value of deflection δ, c_e and c_m become a function of each other., The two unknowns can now be obtained by solving the two equations simultaneously. After obtaining the value of c_e and c_m for a given value of δ, then

N, M_e and M_m can be obtained consequently, and thereafter the load capacity P can be obtained from equation (12).

Equations (20) and (24) can be solved iteratively using appropriate mathematical programming software. Starting with a deflection δ correspond to ultimate concrete strain and yield strain of tension steel bars and increasing δ gradually, the values of c_e and c_m can be calculated. The starting value of deflection δ can be calculated firstly from the compatibility equation (24), using maximum values for c_e and $c_m$that ensure steel yield and ultimate concrete strain. Maximum values for c_e and $c_m$can be calculated from equation (7) by putting $\varepsilon_s = \varepsilon_y$, as follows:

$$c_{e(\max)} = c_{m(\max)} = \frac{d\,\varepsilon_{cu}}{\varepsilon_y + \varepsilon_{cu}} \qquad (25)$$

It should be mentioned that the starting step of the iteration process is not the actual peak value of the load capacity at CAA. During the progress of the iteration process, the values of c_e and c_m take the exact values until $N_e = N_m$ and then the peak load *P* obtained.

Determination of bar fracture

In order to obtain the deflection δ corresponding to bar fracture, the strain in the tension steel bars should be monitored for each increment of deflection δ. From the experimental results and observations, the fracture of top or bottom bars during CAA causes the beam section to lose its ability to carry the loads by flexural action. The beam section carries the load after bar fracture by pure tension either by the top or bottom bars. This indicates that bar fracture at both sides, either at the ends or at the middle joint, will be followed by the onset of the catenary action stage.

There are two possible scenarios for the sequence of bar fracture. The first scenario is that top steel bars at the beam ends fracture first followed by the onset of catenary action and then fracture of bottom steel bars at the middle joint will occur during the catenary action stage. The second scenario is that the bottom steel bars at the middle joint fracture first followed by onset of catenary action and then fracture of the bottom steel bars at the middle joint will occur during catenary action stage.

In Figure (9), which shows the two possible scenarios, δ_{Ft} , δ_{Fb} represent the deflections at which top and bottom fracture respectively, and δ_D represents the deflection at the onset of catenary action stage.

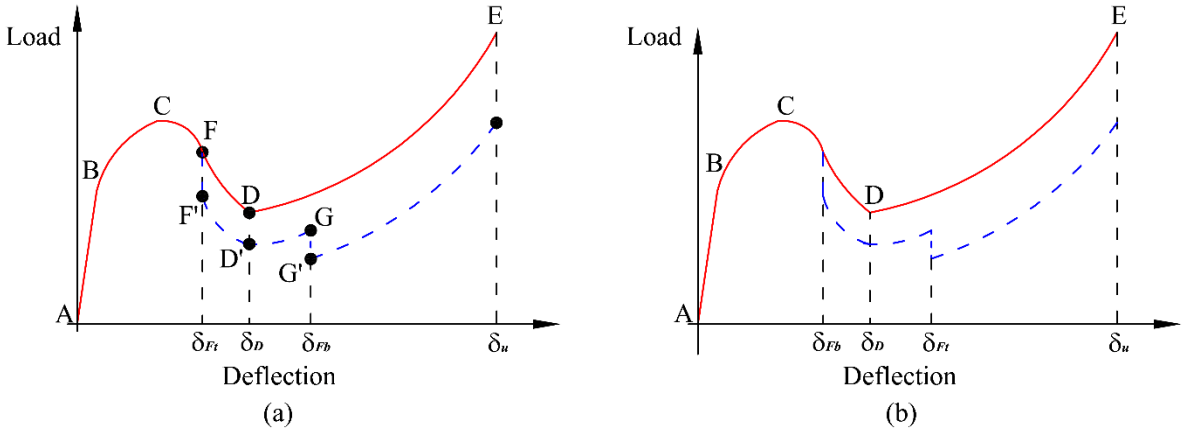

Figure 9: Possible scenarios for bar fracture (a) first scenario and (b) second scenario

From Figure (8), the steel bar elongations l_e and l_m can be calculated as follows:

$$\sin(\theta) = \frac{l_e}{d_i - c_e} = \frac{l_m}{d_i - c_m} \tag{26}$$

$$\sin(\theta) = \frac{\delta}{L - c_m \tan(\theta) + (h - c_e)\tan(\theta)} \tag{27}$$

By equating equations (26) and (27) and arranging the parameters:

$$l_e = \frac{\delta(d_i - c_e)L}{L^2 + \delta(h - c_e - c_m)} \tag{28}$$

$$l_m = \frac{\delta(d_i - c_m)L}{L^2 + \delta(h - c_e - c_m)} \tag{29}$$

It is known from the mechanics of materials that the strain is equal to the elongation divided by the original length. According to the assumption of perfect bond between concrete and steel bars, the length that experiences the elongation is the plastic hinge length only.

Many researchers have attempted to obtain the length of plastic hinge in RC beams and columns. According to Mattock (Mattock, 1965) , the length of the plastic hinge can be obtained from the empirical formula as follows:

$$l_p = 0.5d + 0.05z \tag{30}$$

Where z is the distance from the point of maximum moment to the point of zero moment.

Therefore, the strain can be calculated as follows:

$$\varepsilon_{se} = \frac{l_e}{l_p} \tag{31}$$

$$\varepsilon_{sm} = \frac{l_m}{l_p} \tag{32}$$

For each deflection increment, the strains ε_{se} and ε_{sm} are calculated using equations (28) to (32), then the results are compared with ultimate steel strain. If one of the calculated strains ($\varepsilon_{se}\ or\ \varepsilon_{sm}$) equals or exceeds the ultimate steel strain this means that the steel bars at that section are fractured and the beam carries the load by means of catenary action.

By following the steps shown in figure 10, the relationship between the applied load and the middle joint deflection can be obtained. The first step in the flowchart requires input of all material, geometry and boundary condition properties. The loop (i) is an iterative process to find the correct solution for values of c_e and c_m when $N_e = N_m$, and the loop (j) implements the gradual increase of the deflection. The deflection increment can be used as a percentage of the beam height such as $0.1h$ or $0.05h$ which depends on the accuracy required. At the deflection correspond to the steel bar fracture (Point F'), the moment capacity at that section will be equal to zero. The load corresponding to steel bar fracture can be calculated using equation 12 by taking either M_e or M_m to be zero, which depends on whether the fracture has occurred.

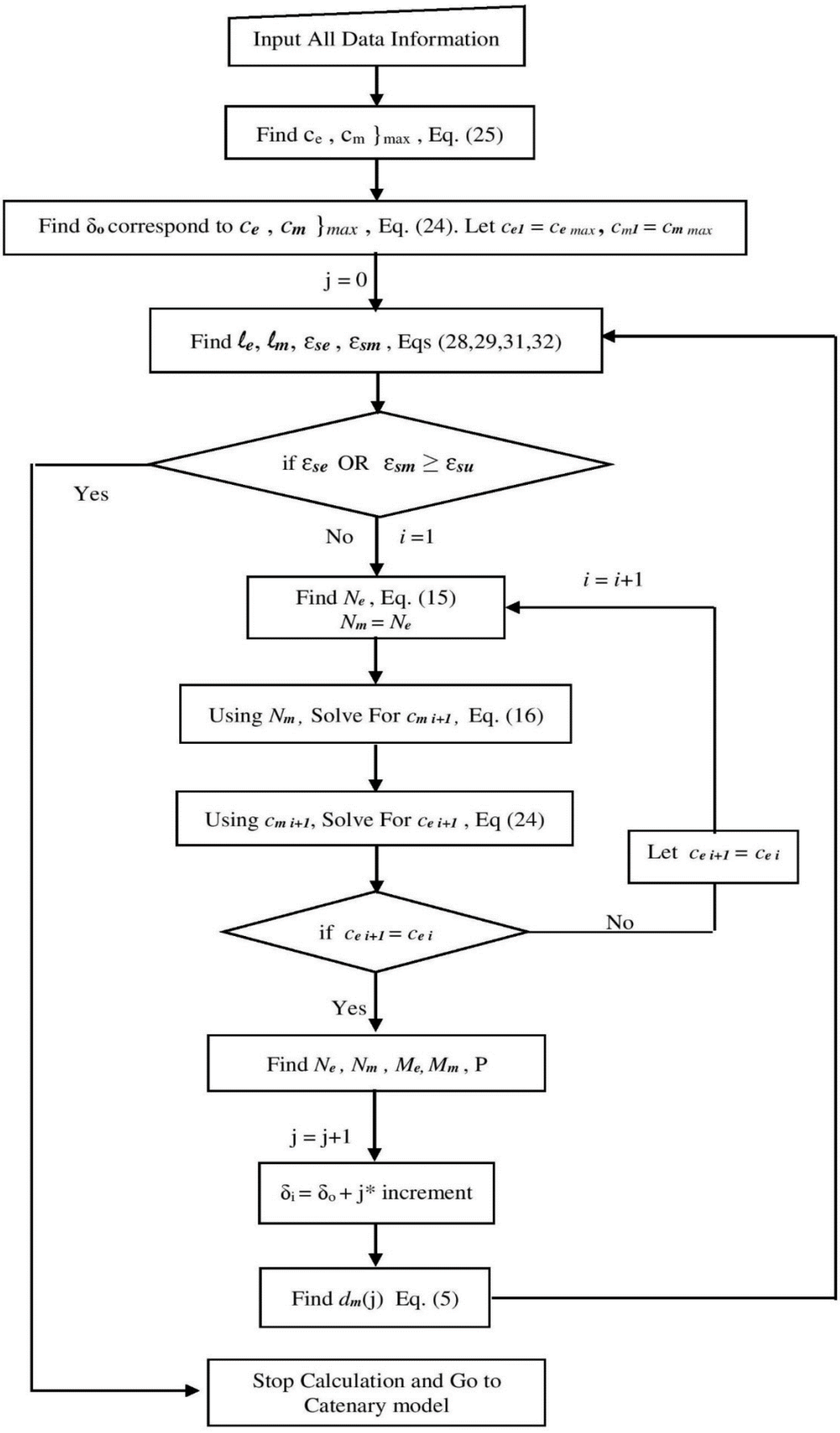

Figure 10: Flowchart of the steps to implement the process of CAA.

Development of the Catenary Model

There are two possible scenarios for bar fracture. The first scenario is that the tension steel bars at the beam ends fracture first followed by the onset of catenary action, or tension steel bars at the middle joint fracture first.

Both scenarios can follow the same steps to obtain the structural behaviour at catenary action stage. After the fracture of steel bars at the middle joint or at the beam ends, the load will be carried by the remaining steel bars by means of tensile forces, which were previously carrying the loads by means of compressive forces during CAA.

Transition from compression to tension means that there is a zero point of axial force that indicates the onset of catenary action at a deflection δ_D as shown in Figure 9(a). On the other hand, the load will be carried by means of flexure at the intact joint where no bar fracture occurred. As the deflection increases, the beam force increases in axial tension, and the tensile forces in the tension steel bars at the intact joint increases and eventually fractures at a deflection δ_{Fb}. As the deflection increases beyond δ_{Fb}, the load will be carried by axial tension throughout the beam length.

The tensile force at the beam end may not represent the actual tensile forces in all sections due to concrete confinement and formation of plastic hinges at the critical sections. In order to simplify the calculation, it is assumed a uniform axial force will be developed along the length of the beam. During catenary action, there are three critical points, as shown in Figure 9, and they are; the catenary action start point D, steel bar fracture G, and ultimate load capacity E.

Figure 11 shows a single bay beam after fracture of the tension steel bars at the beam end. During catenary action and under tensile axial forces, the end supports are expected to move onwards for a distance (u), which depends on the surrounding stiffness.

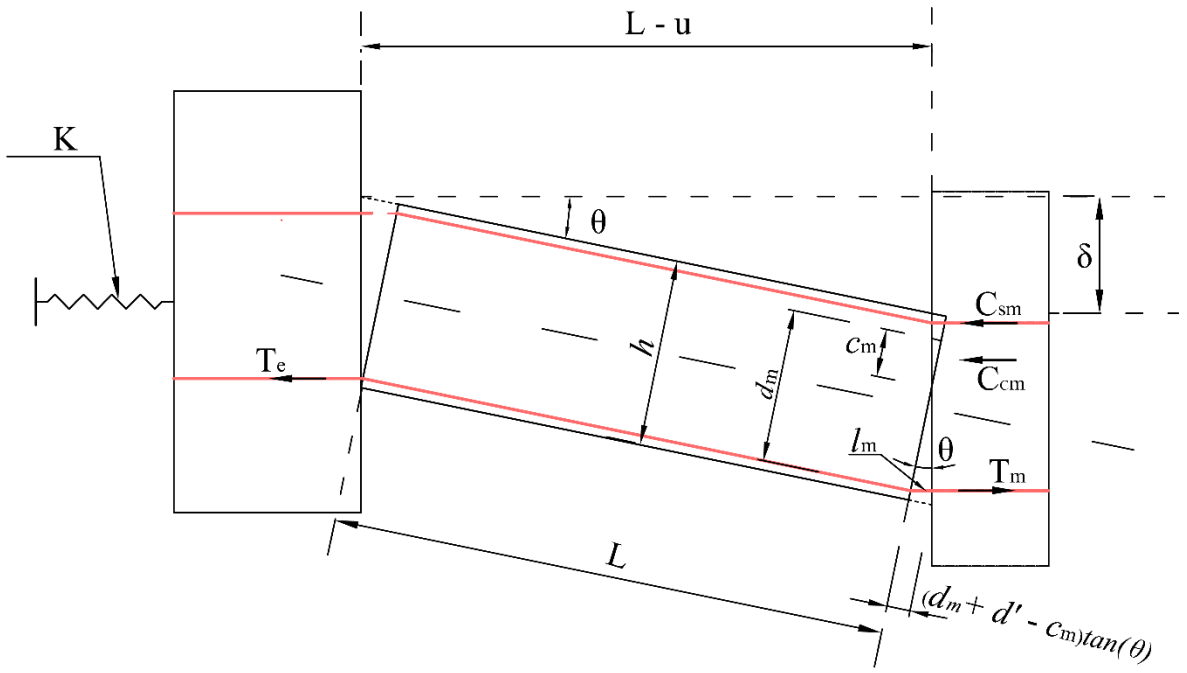

Figure 11: Deflected shape of a single bay beam after bar fracture at the beam end.

In order to determine the catenary action start point which occurs at a deflection δ equal to δ_D, two equations are required to be developed and solved for the two unknowns δ_D and c_m. At the onset of catenary action, the axial force will be equal to zero, therefore, the equilibrium equation will be as follows:

$$C_{cm} + C_{sm} - T_m = 0 \tag{33}$$

Substituting equations (17, 18, 19) into equation (33):

$$0.85 f_c' b \beta c_m + \varepsilon_{sm}' E_s A_{sm}' - f_s A_{sm} = 0 \tag{34}$$

Since ε_{sm}' is a function of δ_D, the equation (34) has two unknowns, which are; δ_D and c_m. For the compatibility equation, the movement of the support (u) at the onset of catenary action will be zero due to $N = 0$. From Figure (11) and triangular geometry, the relationship between δ_D and c_m can be derived as follows:

$$\delta_D^2 + L^2 = (L + (d_m + d' - c_m)\, tan(\theta))^2 \tag{35}$$

By rearranging equation (35) and substituting $tan(\theta) = \delta_D / L$, equation (35) will be as follows:

$$\delta_D = \frac{2(d_m + d' - c_m)L^2}{L^2 - (d_m + d' - c_m)^2} \quad (36)$$

By solving equations (34) and (36) simultaneously, δ_D and c_m values can be found. Thereafter, C_{cm} and C_{sm} can be obtained, and with these values in hand, M_m can be obtained from equation (14). Finally, the load P can be obtained from equation (12), with M_e and N equal to zero.

The second critical point in the CTA stage is the fracture of tension steel bars at the middle joint, which is point G in Figure 9. After the onset of catenary action and as the deflection increases, the beam develops a tensile axial force. At the middle joint, the internal compressive forces decrease and the tensile force increases until the fracture of the tension steel bars occurs. At the fracture of tension steel bars of the middle joint, the compressive forces change abruptly into tensile force.

It is expected at early stages of catenary action, the axial tensile force developed is small, and the tension steel bars at the middle joint are at an advanced stage of yielding. Therefore, it is expected that the axial inward movement of the supports (u) is extremely small compared with L, and can be neglected to simplify the calculation.

From Figure (12) which shows the triangular deflected shape of the beam after the fracture of top bars at the beam end, δ_{Fb} can be obtained as follows:

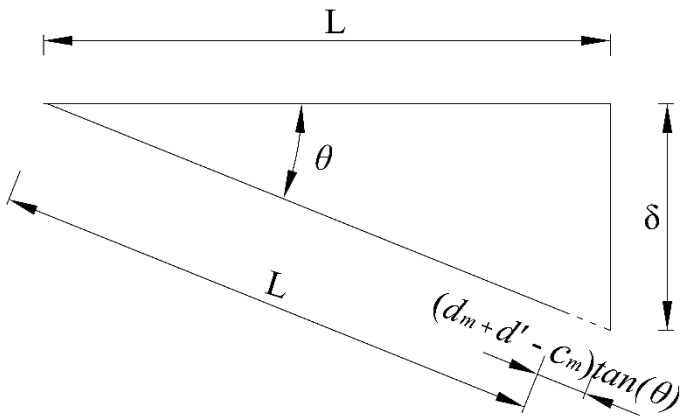

Figure 12: Deflected shape of the beam after top bar fracture at the beam end

$$sin(\theta) = \frac{\delta}{L + (d_m + d' - c_m)tan(\theta)} \quad (37)$$

Equating with equation (26) and rearranging, the relationship between δ and c_m is as follows:

$$\delta = \frac{l_m L^2}{L(d_m - c_m) - l_m(d_m + d' - c_m)} \quad (38)$$

At the fracture point, the strain of the tension steel bars will be equal to the ultimate steel strain. Therefore, from equation (30), the steel elongation l_m at which bar fracture occurs can be obtained as follows:

$$l_m = \varepsilon_{su} l_p \quad (39)$$

By substituting equation (39) into equation (38):

$$\delta_{Fb} = \frac{\varepsilon_{su} l_p L^2}{L(d_m - c_m) - \varepsilon_{su} l_p(d_m + d' - c_m)} \quad (40)$$

Equation (40) relates two unknowns, δ_{Fb} and c_m. Another equation is required to solve for these variables, which is equation (36) and can be written as follows:

$$\delta_{Fb} = \frac{2(d_m + d' - c_m)L^2}{L^2 - (d_m + d' - c_m)^2} \quad (41)$$

By solving equations (40) and (41) simultaneously, the load capacity *P* can be obtained using equation (12) with M_e equal to zero.

Figure (13) shows a single bay beam before total snap-through of the middle joint. After this point, the load *P* is carried only by pure tensile forces. At point G' in figure 9, the line of action of the tensile force acts at an angle φ and magnitude *N* (equal to the tensile force at point G). Therefore, the load *P* at point G' which corresponds to δ_{Fb} can be calculated as follows:

$$P = 2N\sin(\varphi) \quad (42)$$

$$\sin(\varphi) = \frac{\delta_{Fb} - (d - d')\cos(\theta)}{\sqrt{L^2 + (d - d')^2}} \quad (43)$$

$$\cos(\theta) = \cos\left(\tan^{-1}\frac{\delta_{Fb}}{L - u}\right) = \frac{L - u}{\sqrt{\delta_{Fb}^2 + (L - u)^2}} \quad (44)$$

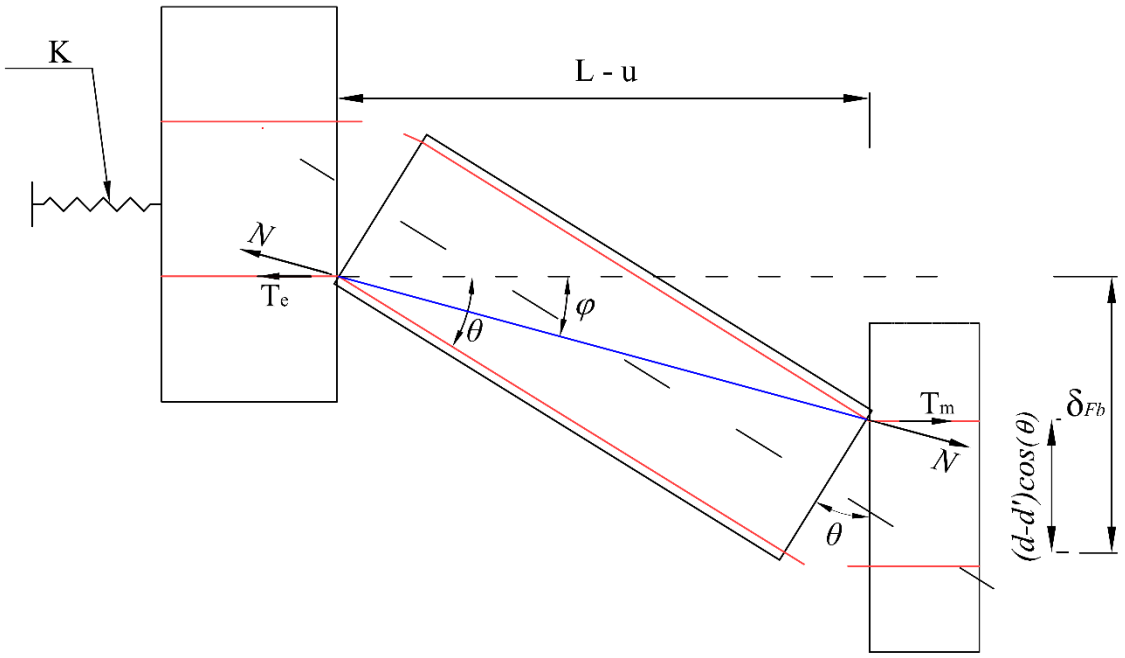

Figure 13: Deflected shape of single bay beam after second bar fracture.

The final critical point (E') at the CTA stage is the ultimate capacity which corresponds to the deflection δ_u. As the applied load increases beyond the load corresponding to the second bar fracture, the vertical deflection increases until the longitudinal steel bars attain their full strain capacity and eventually fracture. Figure (14) shows the deflected shape of the double bay beam at second bar fracture and at ultimate state. From geometry and compatibility conditions, the ultimate deflection δ_u can be obtained as follows:

$$\delta_u = \sqrt{L_2^2 - (L-u)^2} \tag{45}$$

$$L_2 = L_1 + \Delta L \tag{46}$$

$$L_1 = \sqrt{L^2 + (d-d')^2} \tag{47}$$

Where

ΔL is the maximum elongation of the beam during catenary action stage.

In accordance with the assumptions of neglecting tensile strength of concrete and the perfect bond between steel bars and concrete, the steel stress will be distributed over the length of the

plastic hinges only. In addition, the failure mode is expected by bar fracture. Therefore, the maximum beam elongation during catenary action can be obtained as follows:

$$\Delta L = 2\varepsilon_{su} l_p \tag{48}$$

After obtaining the ultimate deflection δ_u, the ultimate load capacity P can be obtained from equilibrium conditions as follows:

$$P = 2Nsin(\theta) \tag{49}$$

$$sin(\theta) = \frac{\delta_u}{L_2} \tag{50}$$

$$N = f_u A_s \tag{51}$$

With the assumption that failure will occur at the weakest section, A_s in equation (51) should be taken as the lesser value of the average of the top and bottom steel reinforcement area at any section along the length of the beam.

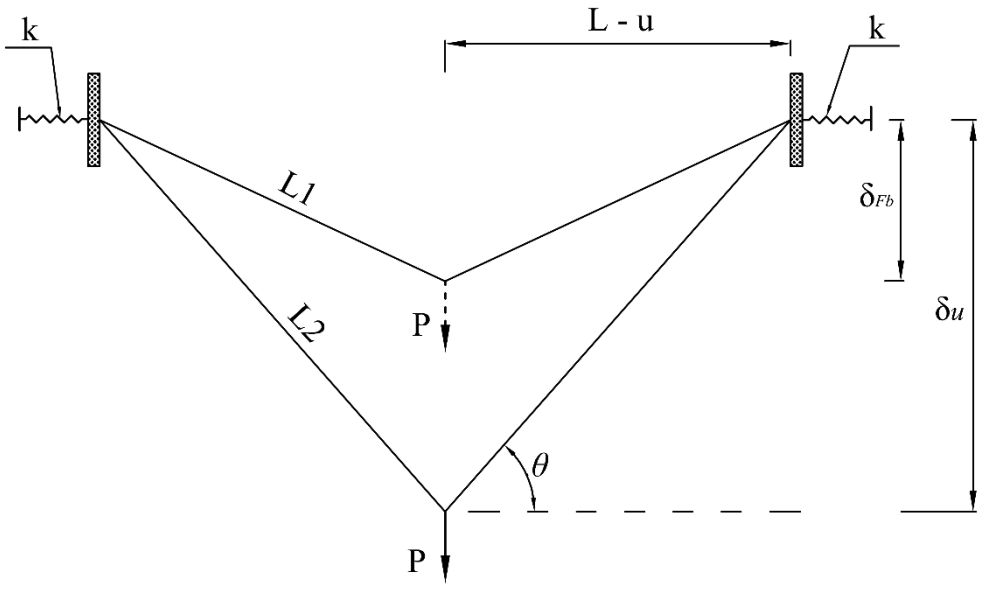

Figure 14: Deflected shape of the double bay beam at second bar fracture and ultimate load

Validation of the Proposed Model

In order to verify the adequacy of the proposed models and equations to predict the structural behaviour of RC beams at CAA and CTA, a comparison with the available test results is performed.

These experiments were performed on RC sub-assemblages consisting of two bay beams and three column stubs. Table 1 lists geometric and material properties of all specimens and compares the theoretical predictions with the experimental test results. In addition, the comparison between theoretical and experimental results are presented graphically as shown in Figure 15. Further information regarding the test results listed in Table 1 can be found in the corresponding papers (Yu and Tan, 2013a, Yu and Tan, 2012, Su et al., 2009, FarhangVesali et al., 2013, Lew et al., 2014, Choi and Kim, 2011).

In order to quantify the relationship between theoretical and experimental results, the correlation factor is obtained, which was 0.987 for the CAA model and 0.940 for the CTA model. In addition, the coefficient of variation is also calculated, which was 0.148 for CAA and 0.265 for the CTA model. The comparison in Table 1 shows that the proposed models at CAA and CTA were able to assess the capacity of RC beams subjected to CRS.

Figure 15 indicates that the CAA model slightly underestimates the capacity of RC beams, while the CTA model slightly overestimates the capacity of RC beams at CTA stage. This can be explained by the occurrence of slip between the concrete and steel reinforcements, which is not considered in the proposed model.

Slip occurrence could allow steel stresses to penetrate through a larger length of steel reinforcement in tension, which cause an increase in CAA load capacity and decrease in the final deflection, leading to an increase in CTA load capacity.

Table 1. Comparison of Experimental and Theoretical results for CAA and CTA models.

No.	Reference	*l/h*	f_c' MPa	Beam Section (mm)		Longitudinal Rein. Ratio (%)		Ultimate capacity (kN)					
								CAA			CTA		
				Width	Depth	Top	Bott.	Exp.	Theo.	Exp./Theo.	Exp.	Theo.	Exp./Theo.
S1	(Yu and Tan, 2013a) & (Yu and Tan, 2012)	11.0	31.2	150	250	0.90	0.49	41.6	38.2	1.089	68.9	67.9	1.015
S2		11.0	31.2	150	250	0.73	0.49	38.4	34.5	1.113	67.6	59.8	1.13
S3		11.0	38.2	150	250	1.24	0.49	54.5	56.8	0.96	124.4	85.9	1.448
S4		11.0	38.2	150	250	1.24	0.82	63.2	66.0	0.958	103.7	100.8	1.029
S5		11.0	38.2	150	250	1.24	1.24	70.3	74.4	0.945	105.1	121.4	0.866
S6		11.0	38.2	150	250	1.87	0.82	70.3	76.1	0.924	143.3	131.6	1.089
S7		8.6	38.2	150	250	1.24	0.82	82.8	83.5	0.992	106.0	114.1	0.929
S8		4.6	38.2	150	250	1.24	0.82	121.3	124.7	0.973	91.8	137.0	0.67
A1	(Su et al., 2009)	4.08	24.5	150	300	0.55	0.55	168.0	140.9	1.192	93.1	110.3	0.844
A2		4.08	26.8	150	300	0.83	0.83	221.0	189.0	1.169	140.0	166.6	0.84
A3		4.08	29.6	150	300	1.13	1.13	246.0	242.3	1.015	178.0	204.9	0.869
A4		4.08	21.9	150	300	0.55	0.38	147.0	128.1	1.148	45.9	72.6	0.632
A5		4.08	25.2	150	300	0.83	0.55	198.0	164.9	1.201	58.1	96.5	0.602
A6		4.08	27.2	150	300	1.13	0.75	226.0	198.6	1.138	144.0	165.8	0.869
B1		6.58	17.6	150	300	1.13	1.13	125.0	117.7	1.062	150.0	149.1	1.006
B2		9.08	18.3	150	300	1.13	1.13	82.9	80.4	1.031	121.0	126.8	0.954
B3		9.08	20.1	150	300	1.13	0.75	74.7	81.6	0.915	90.2	106.5	0.847
C1		6.12	15.1	100	200	1.30	1.30	60.9	45.6	1.336	65.7	78.8	0.834
C2		6.12	16.0	100	200	1.30	1.30	64.9	45.7	1.42	77.6	78.8	0.985
C3		6.12	15.5	100	200	1.30	1.30	68.6	45.6	1.504	54.4	78.8	0.69
V1	(FarhangVesali et al., 2013)	11.72	30.5	180	180	0.51	0.51	40.5	32.4	1.25	12.0	17.8	0.674
V2		11.72	27.0	180	180	0.51	0.51	35.7	31.6	1.13	16.0	17.8	0.899
V3		11.72	30.0	180	180	0.51	0.51	41.4	32.4	1.278	10.0	17.8	0.562
V4		11.72	26.0	180	180	0.77	0.51	40.1	33.7	1.19	16.0	22.3	0.717
V5		11.72	29.5	180	180	0.77	0.51	41.6	34.0	1.224	15.0	22.3	0.673
V6		11.72	30.0	180	180	0.77	0.51	39.4	34.1	1.155	16.0	22.3	0.717
IMF	(Lew et al., 2014)	10.77	32.0	860	660	0.64	0.41	296.0	270.4	1.095	547	538.1	1.017
SMF		7.96	36.0	860	660	0.68	0.59	903.0	810.2	1.115	1232	793.5	1.553
5S	(Choi and Kim, 2011)	6.94	17.0	150	225	1.16	0.46	39.0	36.3	1.074	16.5	48.9	0.337
5G		8.47	17.0	150	185	0.58	0.58	21.0	24.8	0.847	16.5	29.8	0.554
8S		8.01	30.0	140	195	1.46	0.87	54.1	45.2	1.197	84.0	58.2	1.443
8G		9.80	30.0	125	160	0.82	0.82	23.7	23.6	1.004	23.0	30.1	0.764
Mean value of theoretical to experimental ratios									1.114			0.878	
Coefficient of Variation									0.148			0.265	
Correlation coefficient									0.987			0.940	

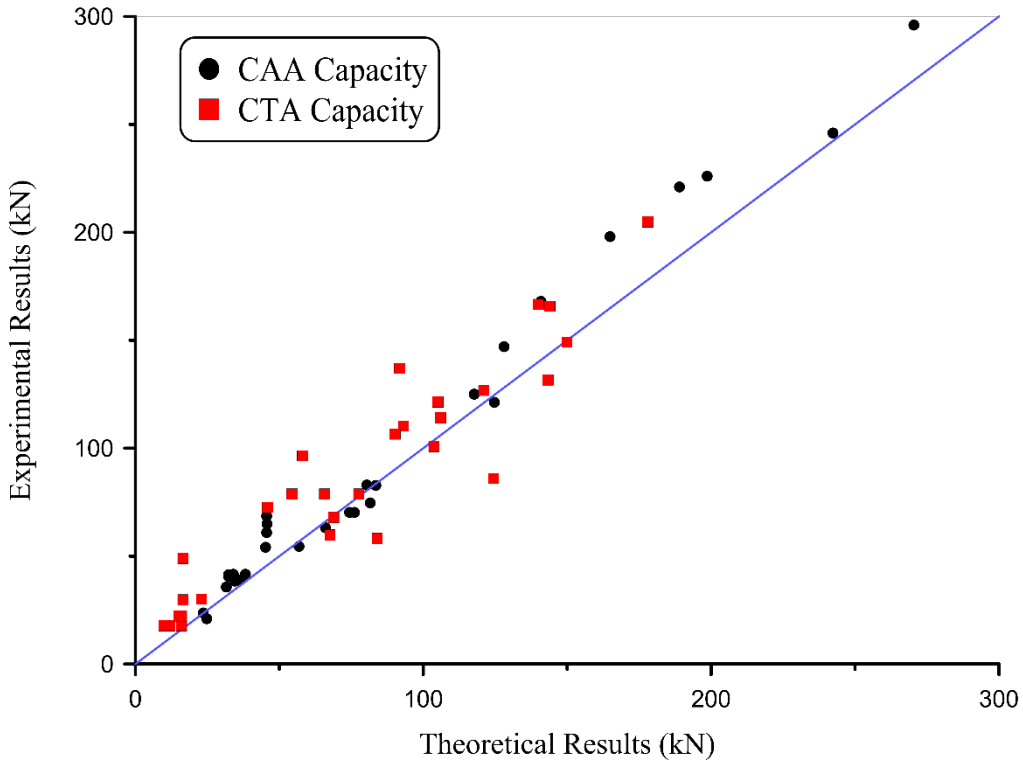

Figure 15 Comparison of experimental and theoretical results for CAA and CTA models.

Another comparison was also made with the test results of an experimental study, which was conducted by the author. The program comprises physical testing of three full scale specimens (SS-1, SS-2 and SS-3). Each specimen comprised of two bay beams and three column stubs. Table 2 shows geometrical and material properties of the tested specimens.

It should be mentioned that during the test of specimen SS-1, the middle joint was not restrained against rotation in the plane of the beam, which resulted in bar fracture at one side with the joint rotating towards this side and the tests was terminated at an early stage of testing.

Table 2. Comparison of experimental and theoretical results for SS-1, SS-2 and SS-3.

No.	*l/h*	f_c' MPa	Beam Section (mm)		Longitudinal Rein. Ratio (%)		Ultimate capacity (kN)					
							CAA			CTA		
			Width	Depth	Top	Bott.	Exp.	Theo.	Exp./Theo.	Exp.	Theo.	Exp./Theo.
SS-1	11.0	28.5	150	250	0.70	0.47	38.5	35.8	1.075	-	36.9	-
SS-2	11.0	28.5	150	250	0.70	0.47	34.9	35.8	0.975	33.2	36.9	0.90
SS-3	11.0	26.8	150	250	0.70	0.47	34.0	33.2	1.024	36.2	36.9	0.981

The comparison between analytical and experimental results of specimen SS-1 and SS-2 are illustrated in Figure 16. Only one analytical curve was obtained for SS-1 and SS-2, this is because material and geometric properties of specimen SS-1 and SS-2 were the same. Figure 17 shows the comparison between analytical and experimental results for specimen SS-3.

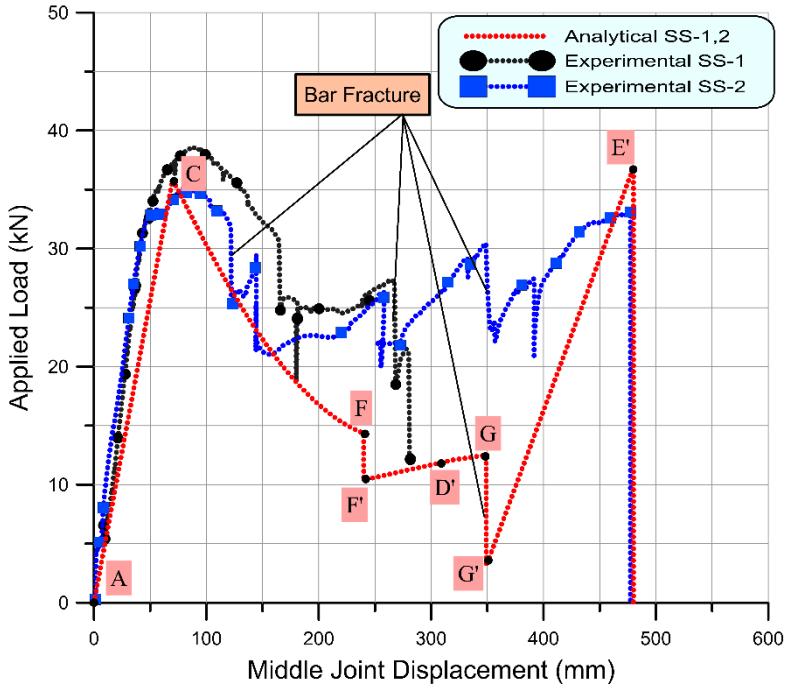

Figure 16: Load-MJD comparison of analytical vs. experimental results for SS-1 and SS-2.

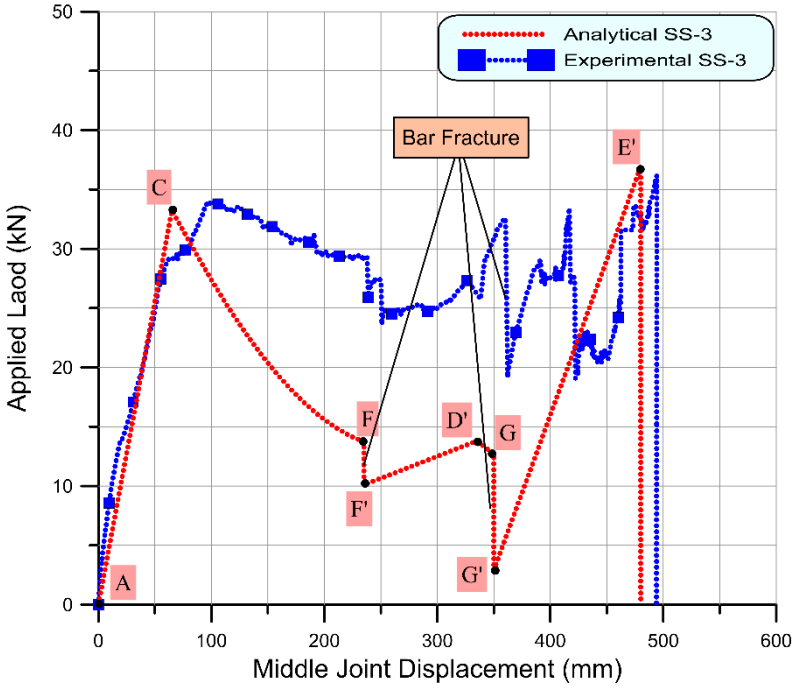

Figure 17: Load-MJD comparison of analytical vs. experimental results for SS-3

It should be noted that the calculation for the CAA model starts with point 'C' shown in figures 16and 17, which represent the ultimate load capacity at CAA. The line AC does not represent the actual elastic behaviour of the RC sub-assemblage as it is drawn to connect the origin with point 'C'.

It can be seen from Figures 16 and 17 that the general trend of both analytical and experimental structural behaviour was quite similar. It is clear from the comparison that the area under the experimental curves are greater than those under the analytical curves. The area under the load-deflection curve represents the strain energy absorbed by a member under any applied load. This means that the analytical model prediction underestimates the progressive collapse capacity of the RC beams.

The analytical model considers that the beam material is of a homogeneous material and regular geometry, also it considers perfect specimen fabrication. For these reasons, the model considers that the fracture of all steel reinforcement within the same layer occurs simultaneously.

The difference between the areas under the analytical and experimental curves could be related to the non-homogeneity of concrete, imperfection of beam construction, steel bar manufacture and unsymmetrical boundary conditions and loading. These parameters clearly affect the experimental results and failure modes such as sequence of bar fracture. Due to the effect of these parameters, the steel bars within the same layer fractured sequentially at different stages of deflection, which is clearly observed during the experimental testing. For ideal and perfect homogeneous conditions, the fracture of all steel bars within the same layer is expected to occur at one specific deflection, which is clearly reflected by the analytical curve.

In fact, the peak demands occur only a very short period of time in the event of progressive collapse. Based on this fact, the fracture of all steel bars at the same layer is likely to happen at the same time. Therefore, it can be concluded that the analytical results represent a lower bound of structural capacity.

Table 3 summarises the forces and their corresponding middle joint displacements at critical stages of load-deflection history for both experimental and analytical results.

It is clear from Table 3 that both experimental and analytical applied load were very close at CAA and CTA. The large difference in load capacity during the transition stage is related to the non-homogeneous conditions in material and geometry as explained earlier in this section.

Also bond slip occurrence during experimental tests explain the larger deflection at peak load in the CAA stage, compared to the deflection obtained analytically in which no consideration for bond slip was taken.

Table 3: Comparison of forces with their MJD's at critical stages

Specimen	Type of Results	Max. load at CAA		At the onset of Catenary Action		Max. Load at Catenary Action	
		P_{com} (kN)	MJD (mm)	P (kN)	MJD (mm)	P_{cat} (kN)	MJD (mm)
SS-1	Experimental	38.5	91.1	26.4	248.3	12.1	280.0
	Analytical	35.8	70.2	12.1	320.0	36.9	497.0
SS-2	Experimental	34.9	89.3	25.2	246.0	33.2	477.3
	Analytical	35.8	70.2	12.1	320.0	36.9	497.0
SS-3	Experimental	34.0	101.0	24.9	272.5	36.2	494.0
	Analytical	33.2	64.9	13.8	335.1	36.9	497.0

Summary and Conclusion

In this paper, an analytical model to predict the structural behaviour of RC beams subjected to column removal has been proposed. Both CAA and CTA are incorporated in this model. The development of the model equations is based on the concepts of equilibrium, compatibility, and material properties. The reduction in beam depth due to concrete crushing, which occurs after the concrete has attained it maximum strain, is also included in this model. During the experimental tests, bar fracture at the middle joint and the beam ends was observed. Therefore, a system of equations has been developed and included in this mode to predict bar fracture and the corresponding load and vertical deflection.

A comparison with the experimental results was conducted and the following summarizes the main findings of this paper:

1. The comparison made between the experimental and analytical results shows the ability of the proposed model to evaluate and predict the structural behaviour of RC beams in the event of progressive collapse.
2. The analytical model is able to predict and evaluate the occurrence of bar fracture at both CAA and CTA. The analytical model considers the beam under investigation with homogenous material and geometry. Based on this, the fracture of all steel reinforcement

in the same layer occurs simultaneously. Although it is rare occurrence in the actual event, it is considered as the worst scenario possible, and the analytical prediction gives the lower bound of progressive collapse capacity.

References

ABBASNIA, R. & NAV, F. M. 2015. A theoretical method for calculating compressive arch capacity of RC beams against progressive collapse. *Structural Concrete,* 17**,** 21-31.

AHMADI, R., RASHIDIAN, O., ABBASNIA, R., MOHAJERI NAV, F. & USEFI, N. 2016. Experimental and numerical evaluation of progressive collapse behavior in scaled RC beam-column subassemblage. *Shock and Vibration,* 2016.

ALASHKER, Y., LI, H. & EL-TAWIL, S. 2011. Approximations in progressive collapse modeling. *Journal of Structural Engineering,* 137**,** 914-924.

ALOGLA, K., WEEKES, L. & AUGUSTHUS-NELSON, L. 2016a. A new mitigation scheme to resist progressive collapse of RC structures. *Construction and Building Materials,* 125**,** 533-545.

ALOGLA, K., WEEKES, L. & AUGUSTHUS-NELSON, L. 2016b. Progressive collapse resisting mechanisms of reinforced concrete structures. *Proceedings of the 5th International Conference on Integrity, Reliability and Failure.* **,** 479-480.

BAO, Y., KUNNATH, S. K., EL-TAWIL, S. & LEW, H. 2008. Macromodel-based simulation of progressive collapse: RC frame structures. *Journal of Structural Engineering,* 134**,** 1079-1091.

CHOI, H. & KIM, J. 2011. Progressive collapse-resisting capacity of RC beam–column sub-assemblage. *magazine of concrete research,* 63**,** 297-310.

DOD 2004. Design of buildings to resist progressive collapse. *Unified Facilities Criteria (UFC)-Deaprtment of Defence*.

EYRE, J. R. 1997. Direct assessment of safe strengths of RC slabs under membrane action. *Journal of Structural Engineering,* 123**,** 1331-1338.

FARHANGVESALI, N., VALIPOUR, H., SAMALI, B. & FOSTER, S. 2013. Development of arching action in longitudinally-restrained reinforced concrete beams. *Construction and Building Materials,* 47**,** 7-19.

GSA 2003. Progressive collapse analysis and design guidelines. *U.S. General Services Administration.*

HASKETT, M., OEHLERS, D. J., ALI, M. M. & WU, C. 2009. Rigid body moment–rotation mechanism for reinforced concrete beam hinges. *Engineering Structures,* 31**,** 1032-1041.

HOU, J., SONG, L. & LIU, H. 2015. Progressive collapse of RC frame structures after a centre column loss. *Magazine of Concrete Research,* 68**,** 423-432.

JIAN, H. & ZHENG, Y. 2014. Simplified models of progressive collapse response and progressive collapse-resisting capacity curve of RC beam-column substructures. *Journal of Performance of Constructed Facilities,* 28**,** 04014008.

KIM, H. 2006. *Progressive collapse behavior of reinforced concrete structures with deficient details,* ProQuest.

KIM, J. & YU, J. 2012. Analysis of reinforced concrete frames subjected to column loss. *Magazine of Concrete Research,* 64**,** 21-33.

LEW, H., BAO, Y., PUJOL, S. & SOZEN, M. A. 2014. Experimental study of reinforced concrete assemblies under column rmoval senario. *ACI Structural Journal,* 111**,** 881-892.

MATTOCK, A. H. 1965. Rotational capacity of hinging regions in reinforced concrete beams. *Special Publication,* 12**,** 143-181.

MEROLA, R. 2009. *Ductility and robustness of concrete structures under accidental and malicious load cases.* The University of Birmingham.

ODPM 2004. Building and Buildings England and Wales-The Building Regulations 2000 No. 2531. *Office of the Deputy Prime Minister*

ORTON, S. 2007. *Development of a CFRP system to provide continuity in existing reinforced concrete structures vulnerable to progressive collapse,* ProQuest.

PARK, R. & GAMBLE, W. L. 1980. *Reinforced concrete slabs,* John Wiley & Sons.

PARK, R. & GAMBLE, W. L. 2000. *Reinforced concrete slabs,* John Wiley & Sons.

POUR, H. V., VESSALI, N., FOSTER, S. & SAMALI, B. 2015. Influence of concrete compressive strength on the arching behaviour of reinforced concrete beam assemblages. *Advances in Structural Engineering,* 18**,** 1199-1214.

QIAN, K. & LI, B. 2015. Load-resisting mechanism to mitigate progressive collapse of flat slab structures. *Magazine of Concrete Research,* 67**,** 349-363.

REGAN, P. 1975. Catenary action in damage concrete structures. *ACI Special Publication,* 48**,** 191-224.

SADEK, F., MAIN, J. A., LEW, H. & BAO, Y. 2011. Testing and analysis of steel and concrete beam-column assemblies under a column removal scenario. *Journal of Structural Engineering,* 137**,** 881-892.

SASANI, M., BAZAN, M. & SAGIROGLU, S. 2007. Experimental and analytical progressive collapse evaluation of actual reinforced concrete structure. *ACI Structural Journal,* 104**,** 731-739.

SU, Y., TIAN, Y. & SONG, X. 2009. Progressive collapse resistance of axially-restrained frame beams. *ACI Structural Journal,* 106**,** 600-607.

YI, W. J., HE, Q. F., XIAO, Y. & KUNNATH, S. K. 2008. Experimental study on progressive collapse-resistant behavior of reinforced concrete frame structures. *ACI Structural Journal,* 105**,** 433-439.

YU, J. & TAN, K.-H. 2013a. Experimental and numerical investigation on progressive collapse resistance of reinforced concrete beam column sub-assemblages. *Engineering Structures,* 55**,** 90-106.

YU, J. & TAN, K. H. 2012. Structural behavior of RC beam-column subassemblages under a middle column removal scenario. *Journal of Structural Engineering,* 139**,** 233-250.

YU, J. & TAN, K. H. 2013b. Special detailing techniques to improve structural resistance against progressive collapse. *Journal of Structural Engineering,* 140**,** 04013077.

YU, J. & TAN, K. H. 2014. Analytical model for the capacity of compressive arch action of reinforced concrete sub-assemblages. *Magazine of Concrete Research,* 66**,** 109-126.

Copyright form

Click here to download Copyright form Signed Copyright form.jpg

Journal Publishing Agreement

It is our policy to ask authors to assign the copyright of articles accepted for publication to the Publisher. Exceptions are possible for reasons of national rules or funding. Please tick the relevant options below.

In assigning copyright to us, you retain all proprietary rights including patent rights, and the right to make personal (non-commercial) use of the article, subject to acknowledgement of the journal as the original source of publication.

By signing this agreement, you are confirming that you have obtained permission from any co-authors and advised them of this copyright transfer. Kindly note that copyright transfer is not applicable to authors who are opting to publish their papers as Open Access. Open Access authors retain copyright of their published paper.

Please complete the form below and return an electronic copy to your ICE Publishing contact: (http://www.icevirtuallibrary.com/info/submit).

Journal name: Magazine of Concrete Research

Article title: Theoretical assessment of progressive collapse capacity of reinforced concrete structures

Manuscript reference number: MACR-D-16-00319

Authors: Kamal Alogla, Laurence Weekes, Leingthan Augusthus-Nelson

Your name: Kamal Alogla, Laurence Weekes, Leingthan Augusthus-Nelson

Signature and date:

Please tick either one option from part A or one option from part B. Please complete part C.

A. Copyright

- [x] I hereby assign and transfer the copyright of this paper to Thomas Telford Ltd.
- [ ] British Crown Copyright: I hereby assign a non-exclusive licence to publish to Thomas Telford Ltd.
- [ ] I am a US Government employee: employed by (name of agency) .....
- [ ] I am subject to the national rules of (country) ..... and confirm that I meet their requirements for copyright transfer or reproduction (please delete as appropriate)

B. Authors with open access funding requirements. Please specify the Creative Commons license version required.

- [ ] CC-BY (for full details click here Creative Commons Attribution (CC BY) 4.0 International License)
- [ ] CC-BY-NC-ND (for full details click here Creative Commons Attribution Non Commercial No-derivatives (CC BY NC ND) 4.0 International License)

C. Please confirm that you have obtained permission from the original copyright holder. For ICE Publishing's copyright policy, please click here. ICE Publishing is a signatory to the STM Guidelines.

- [ ] I have obtained permission from the original copyright holder for the use of all subsidiary material included in this paper (E.g. for borrowed figures or tables).

Thomas Telford Ltd is wholly owned by the Institution of Civil Engineers
ICE Publishing, 1 Great George Street, Westminster, London, SW1P 3AA, UK
Telephone: +44 (0)20 7665 2242 | Fax: +44 (0)20 7665 2189 | Web: www.icevirtuallibrary.com

Figure 1

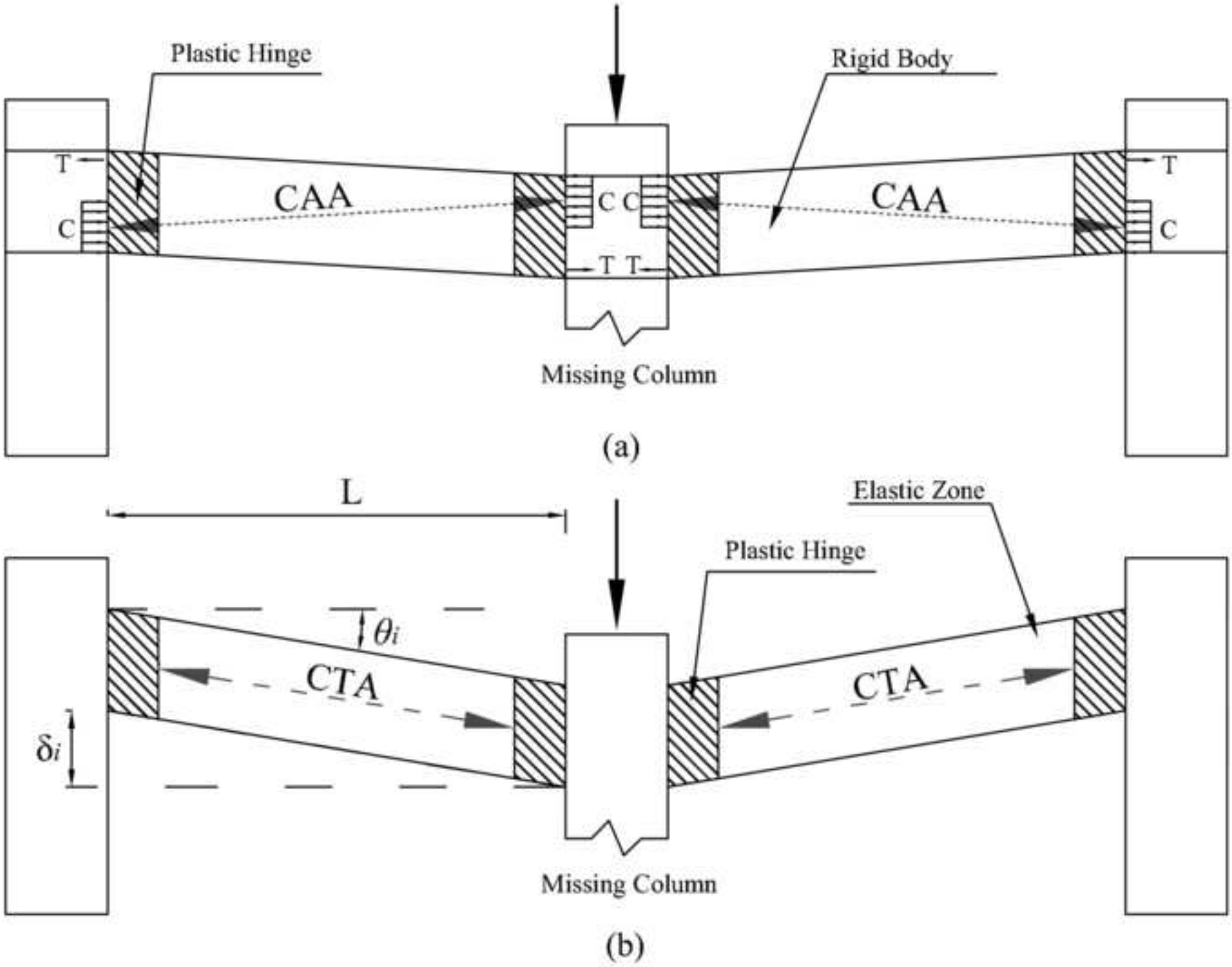

Figure 2

Click here to download Figure 2.tif

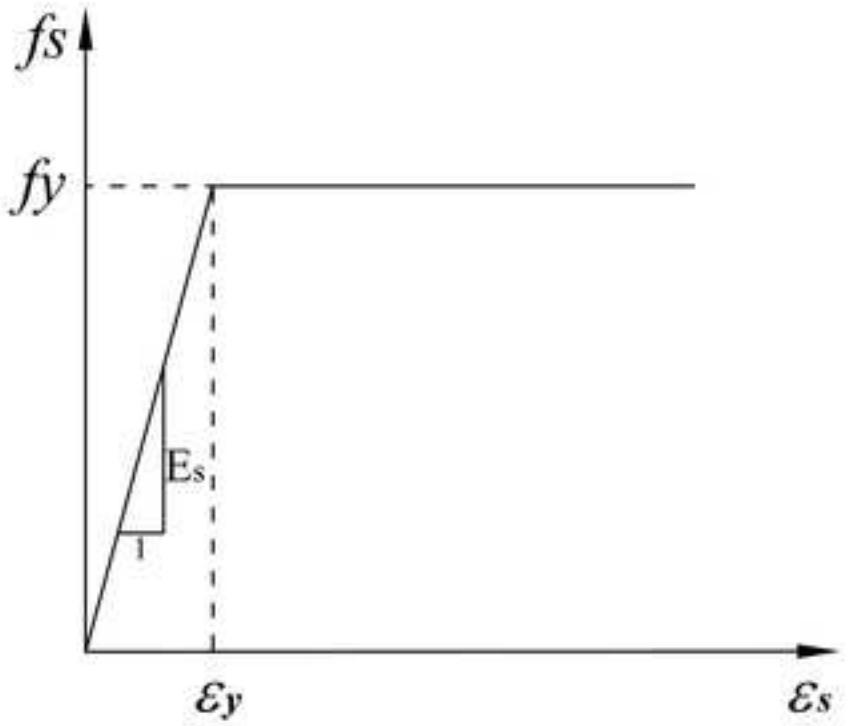

(a)

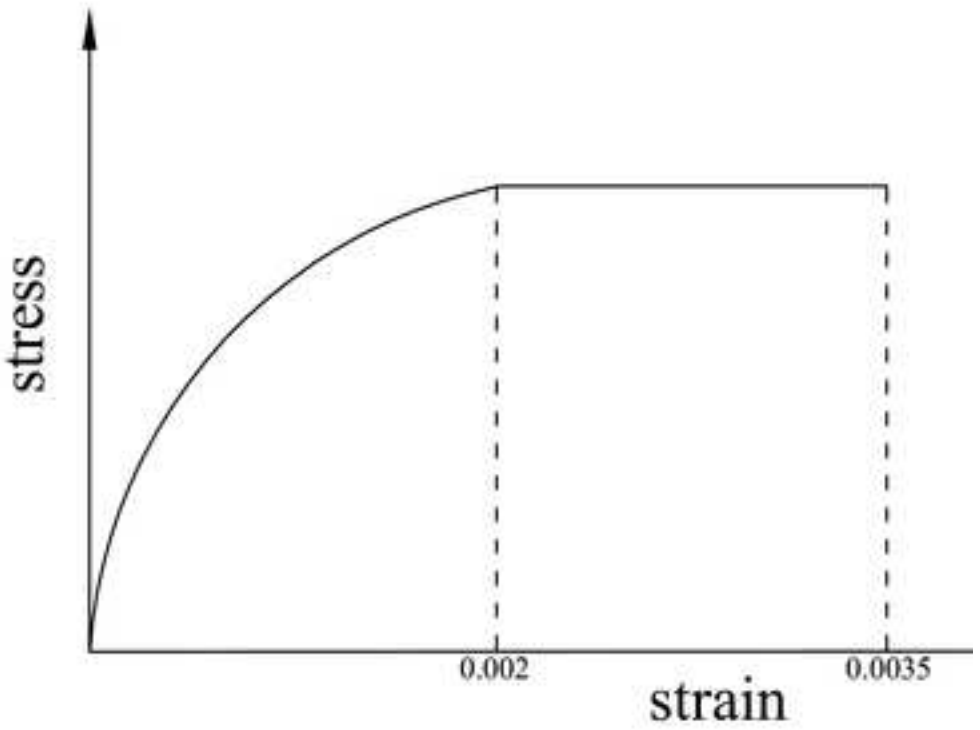

(b)

Figure 3

Click here to download Figure 3.tif

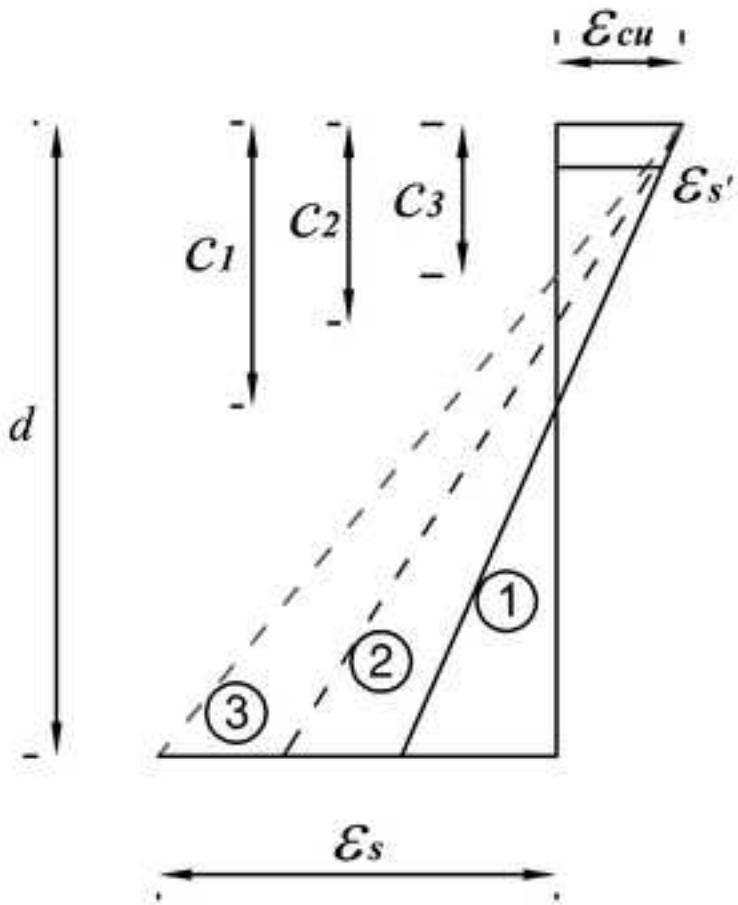

(a)

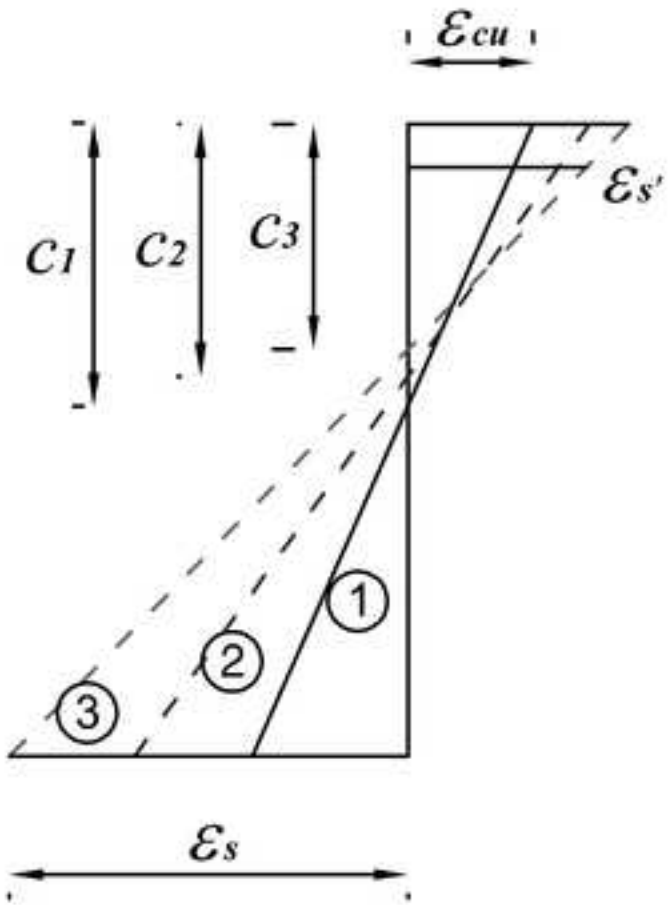

(b)

Figure 4

Click here to download Figure 4.tif

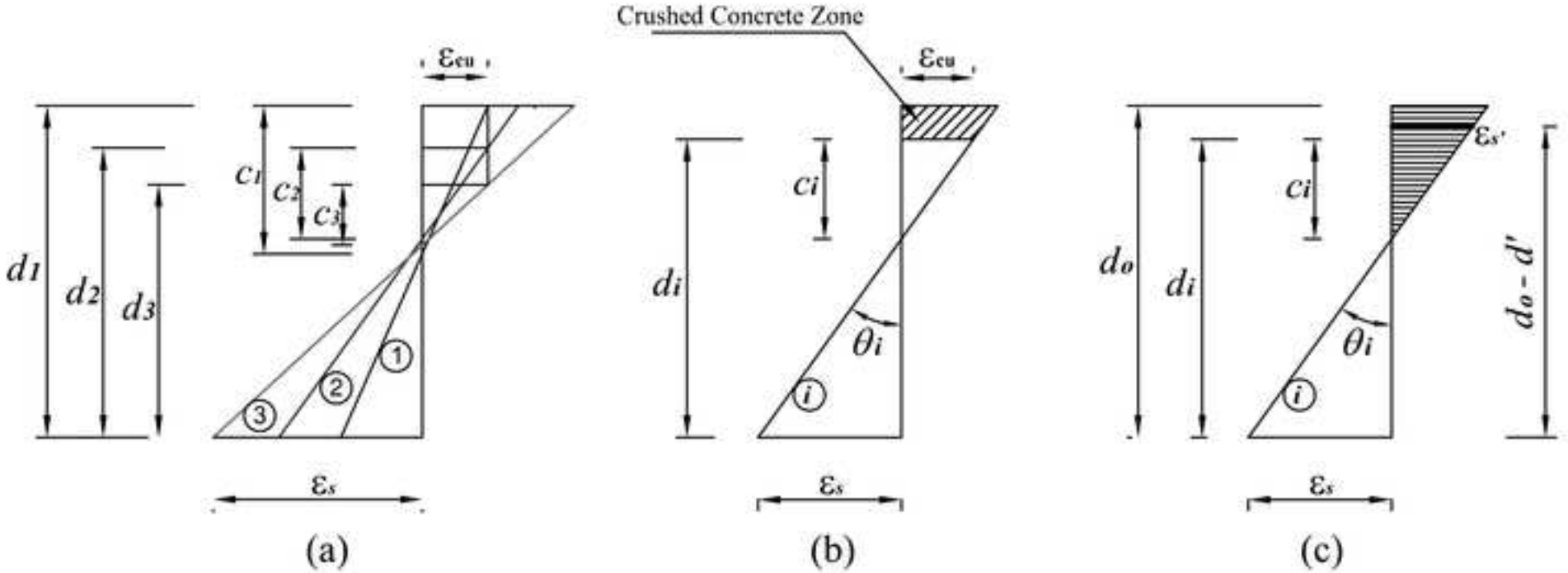

Figure 5

Click here to download Figure 5.tif

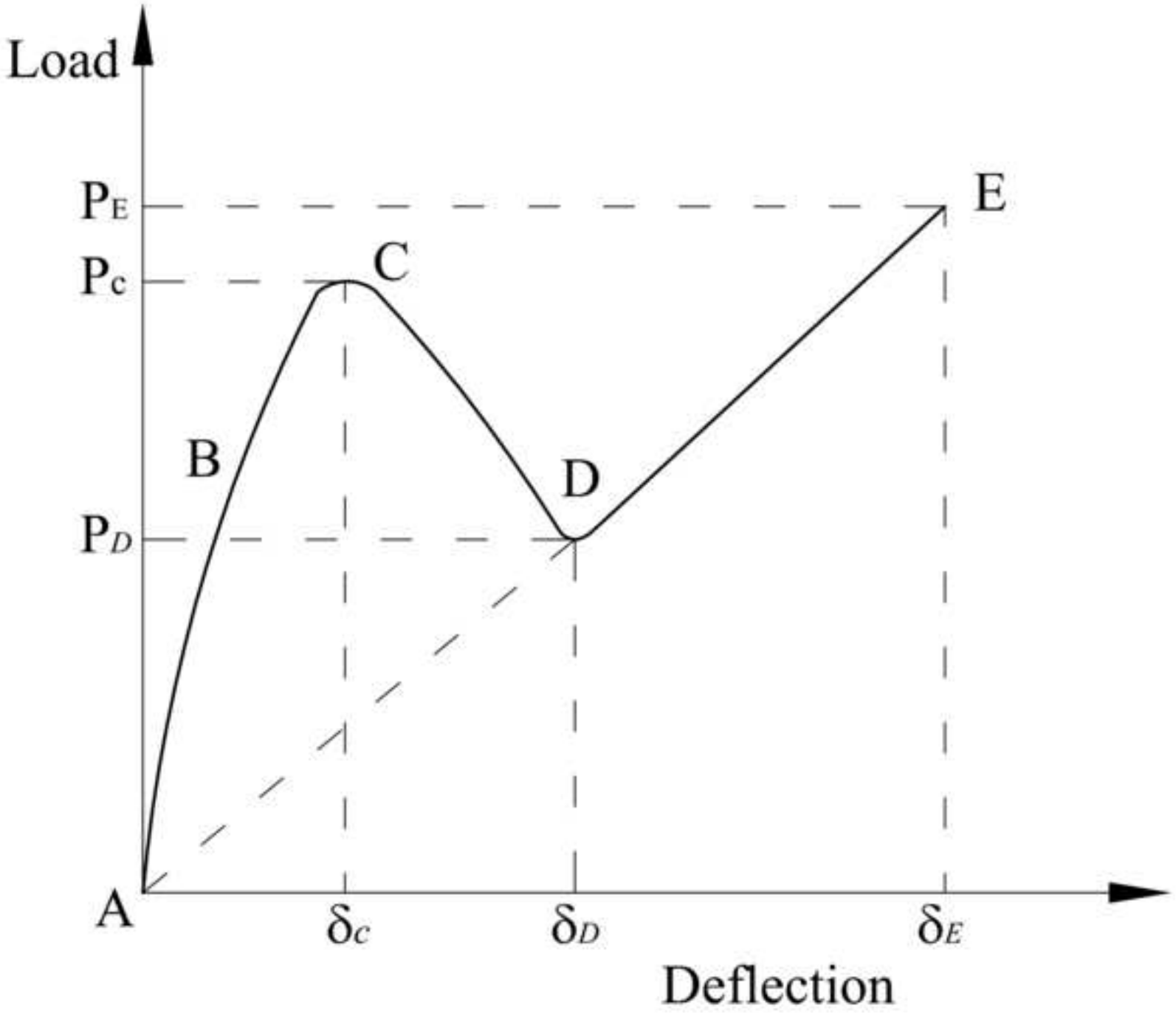

Figure 6

Click here to download Figure 6.tif

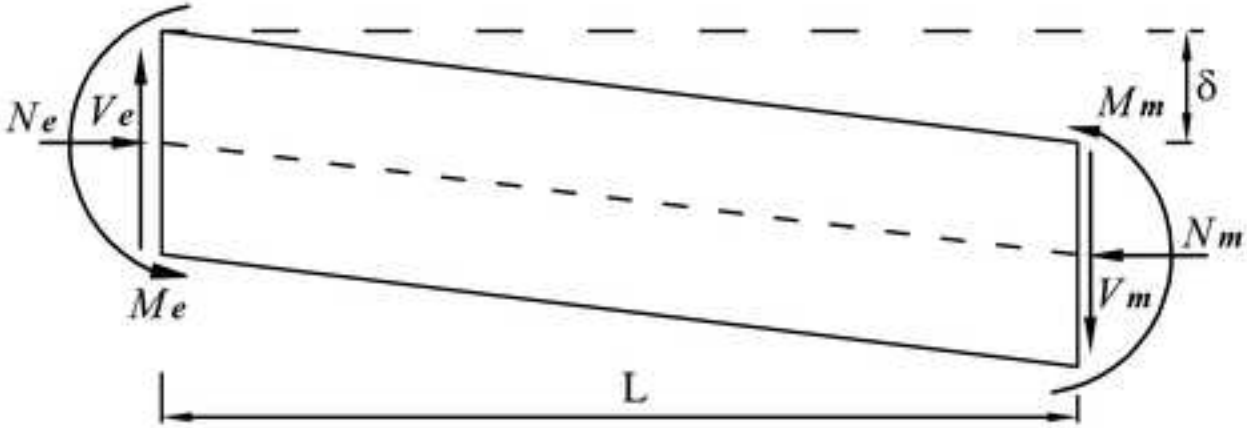

(a) Single Beam

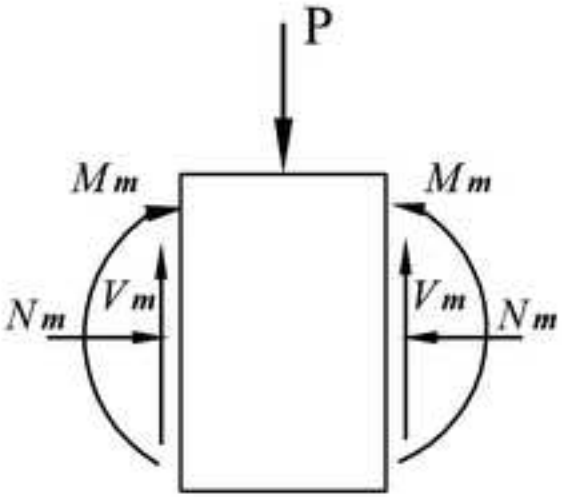

(b) Middle Joint

Figure 7

Click here to download Figure 7.tif

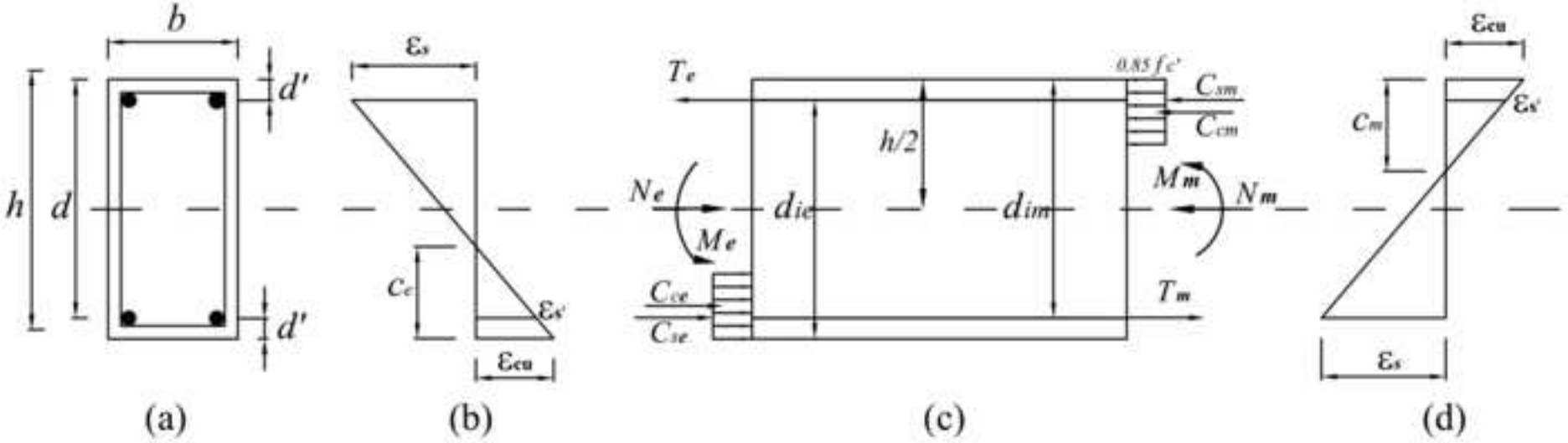

Figure 8

Click here to download Figure 8.tif

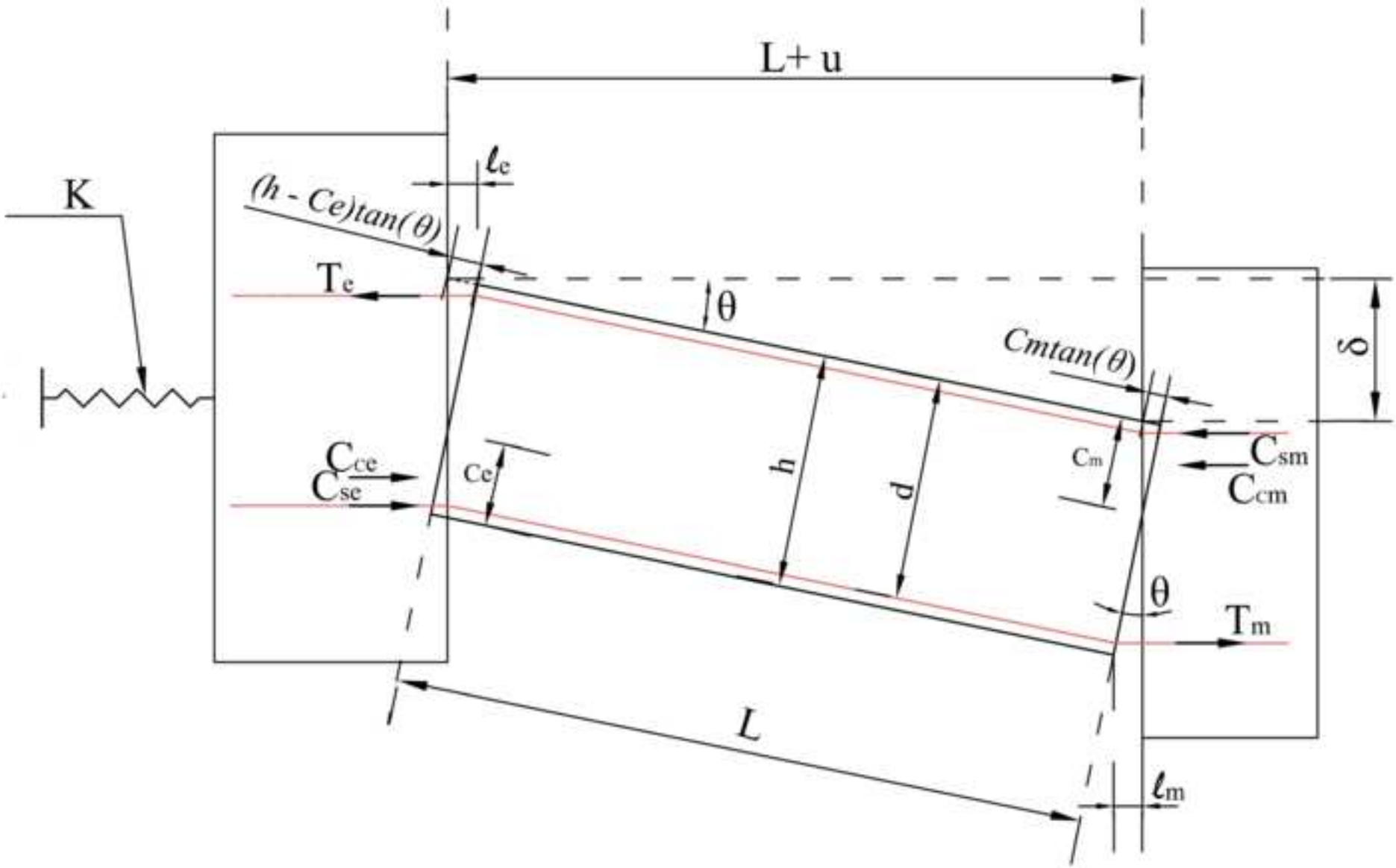

Figure 9

Click here to download Figure 9.tif

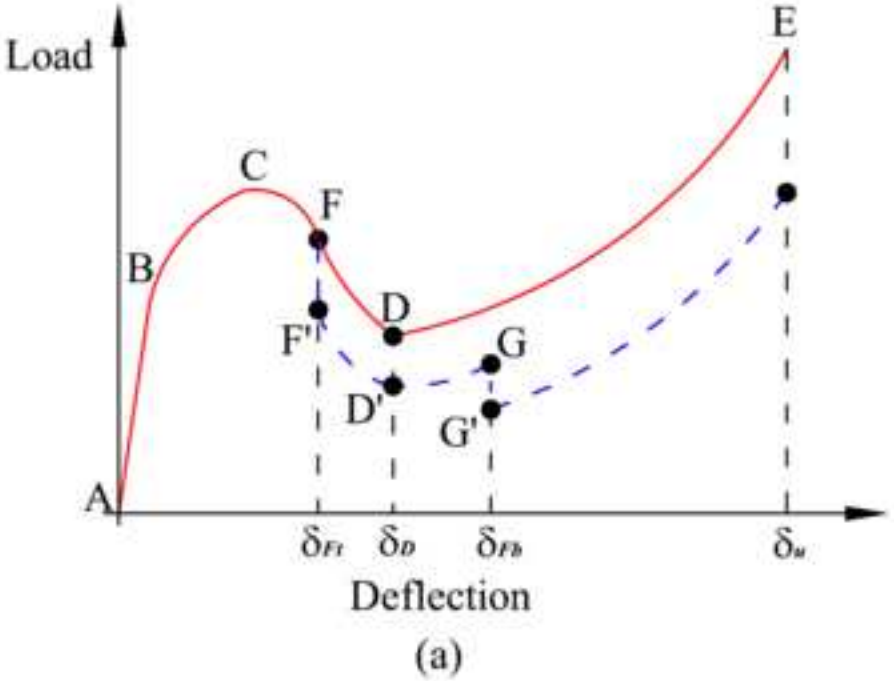

(a)

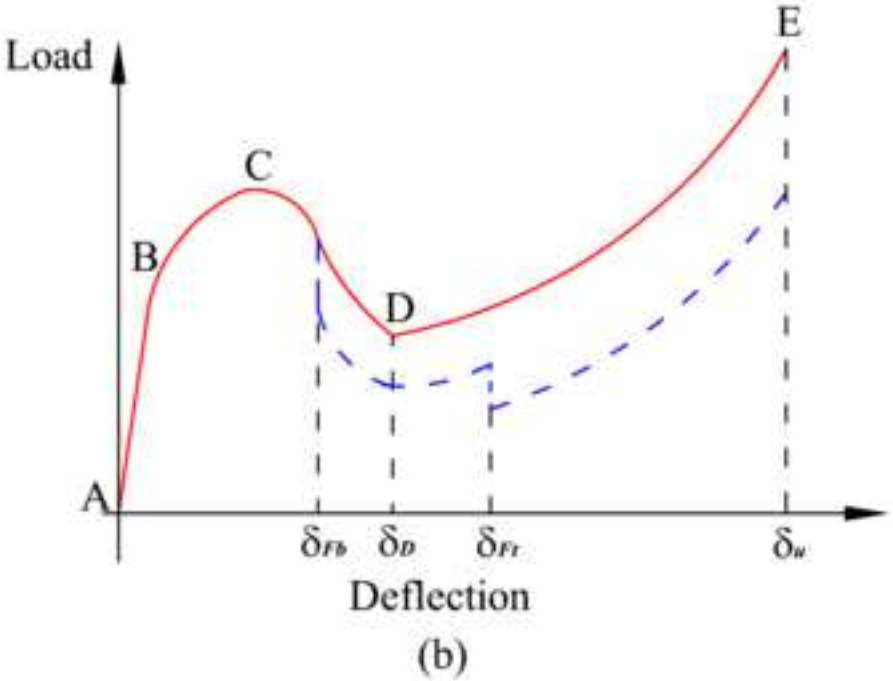

(b)

Figure 10

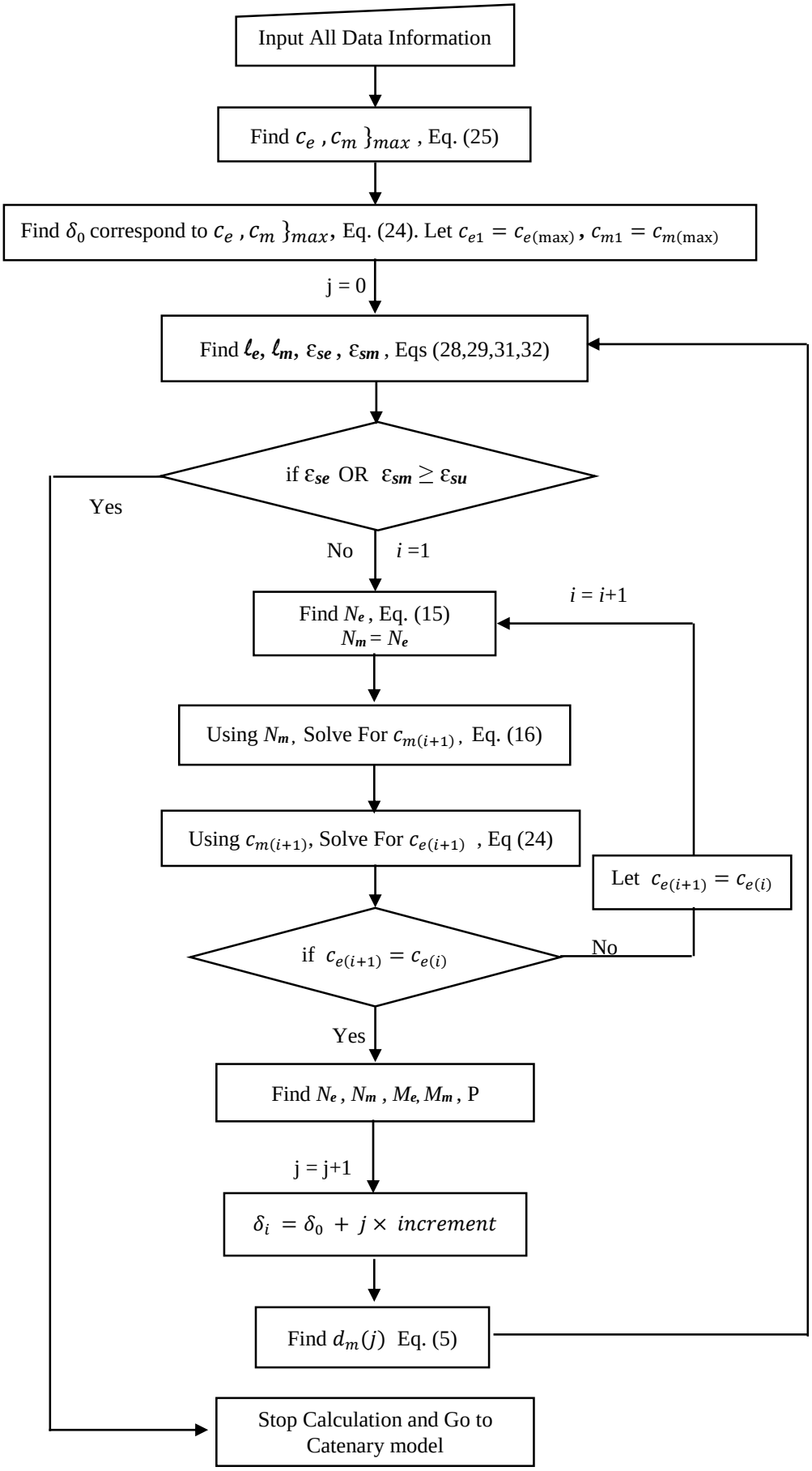
Input All Data Information
Find c_e , c_m $\}_{max}$, Eq. (25)
Find δ_0 correspond to c_e , c_m $\}_{max}$, Eq. (24). Let $c_{e1} = c_{e(\max)}$, $c_{m1} = c_{m(\max)}$
j = 0
Find ℓ_e, ℓ_m, ε_{se} , ε_{sm} , Eqs (28,29,31,32)
if ε_{se} OR $\varepsilon_{sm} \geq \varepsilon_{su}$
Yes
No
i =1
i = i+1
Find N_e , Eq. (15)
$N_m = N_e$
Using N_m, Solve For $c_{m(i+1)}$, Eq. (16)
Using $c_{m(i+1)}$, Solve For $c_{e(i+1)}$, Eq (24)
Let $c_{e(i+1)} = c_{e(i)}$
if $c_{e(i+1)} = c_{e(i)}$
No
Yes
Find N_e , N_m , M_e, M_m , P
j = j+1
$\delta_i = \delta_0 + j \times increment$
Find $d_m(j)$ Eq. (5)
Stop Calculation and Go to Catenary model

Figure 11

Click here to download Figure 11.tif

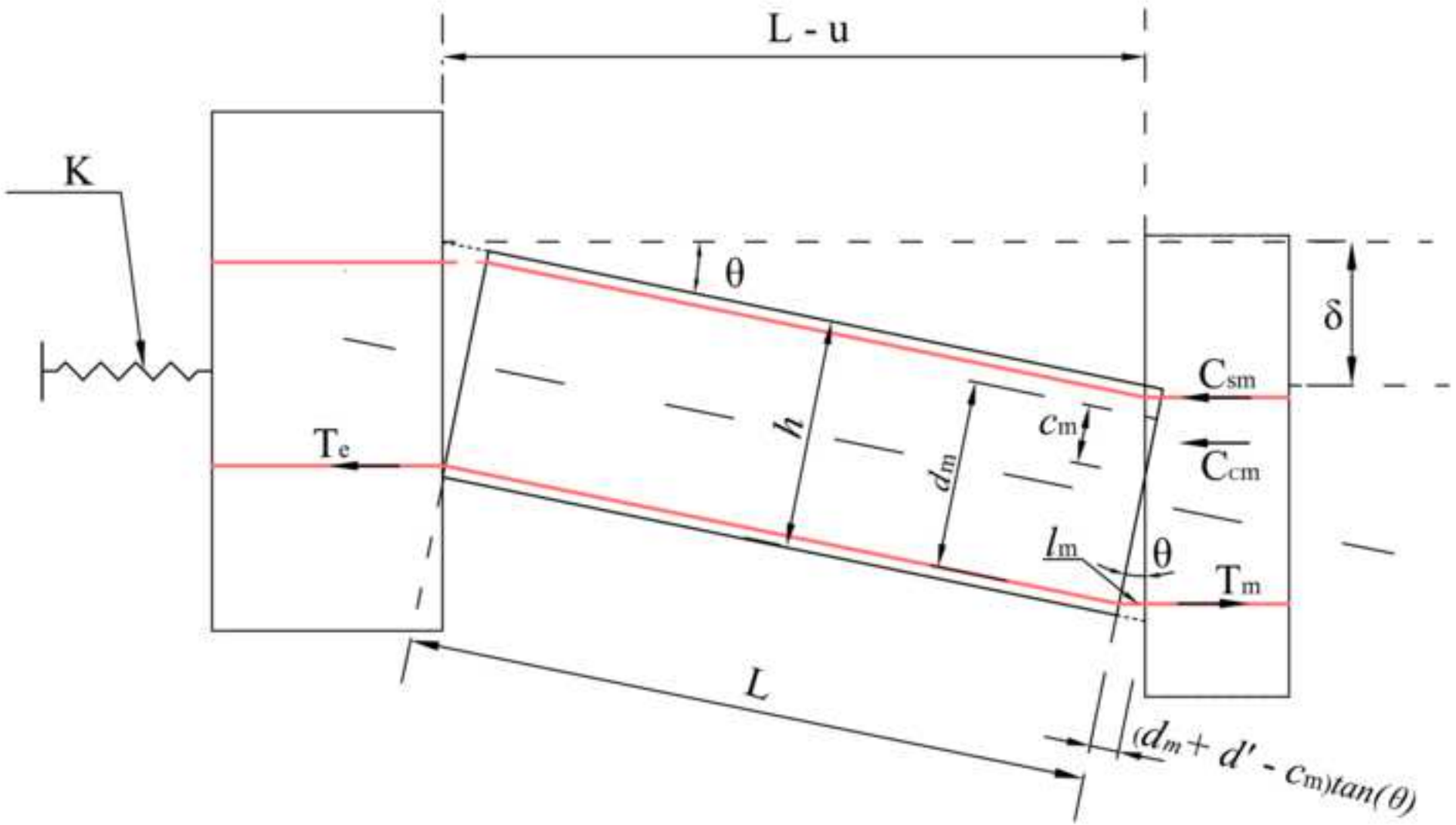

Figure 12

Click here to download Figure 12.tif

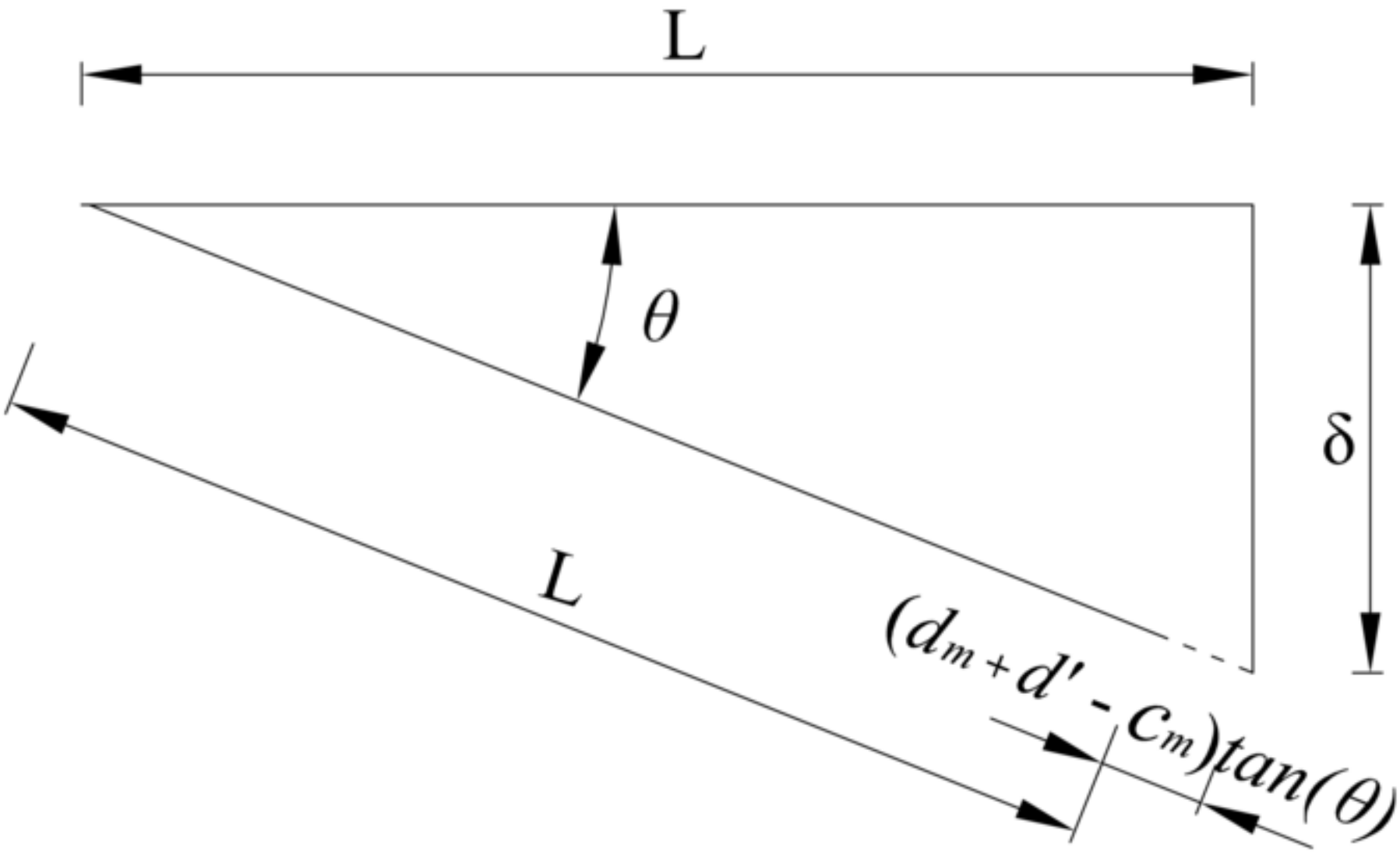

Figure 13

Click here to download Figure 13.tif

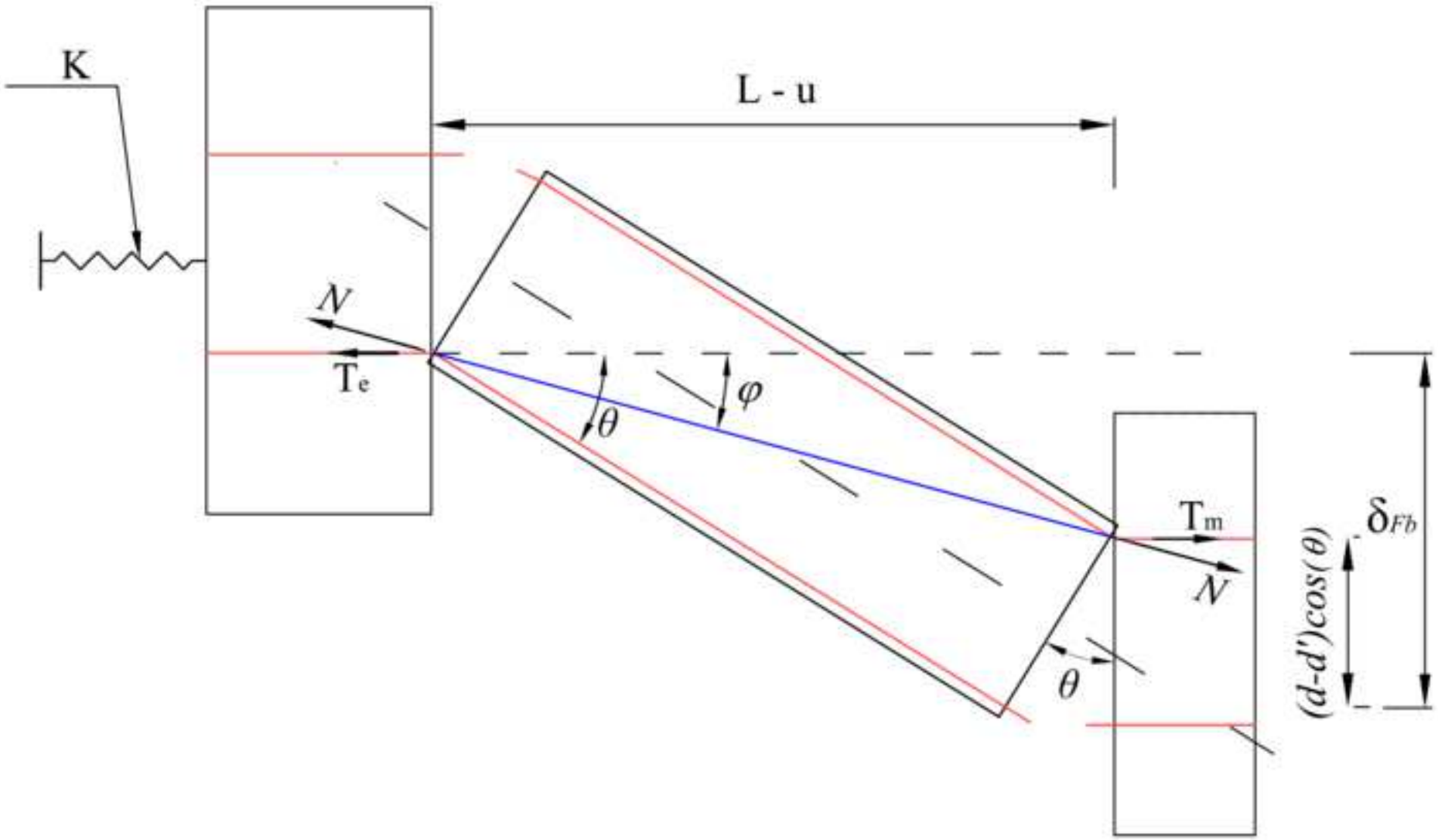

Figure 14

Click here to download Figure 14.tif

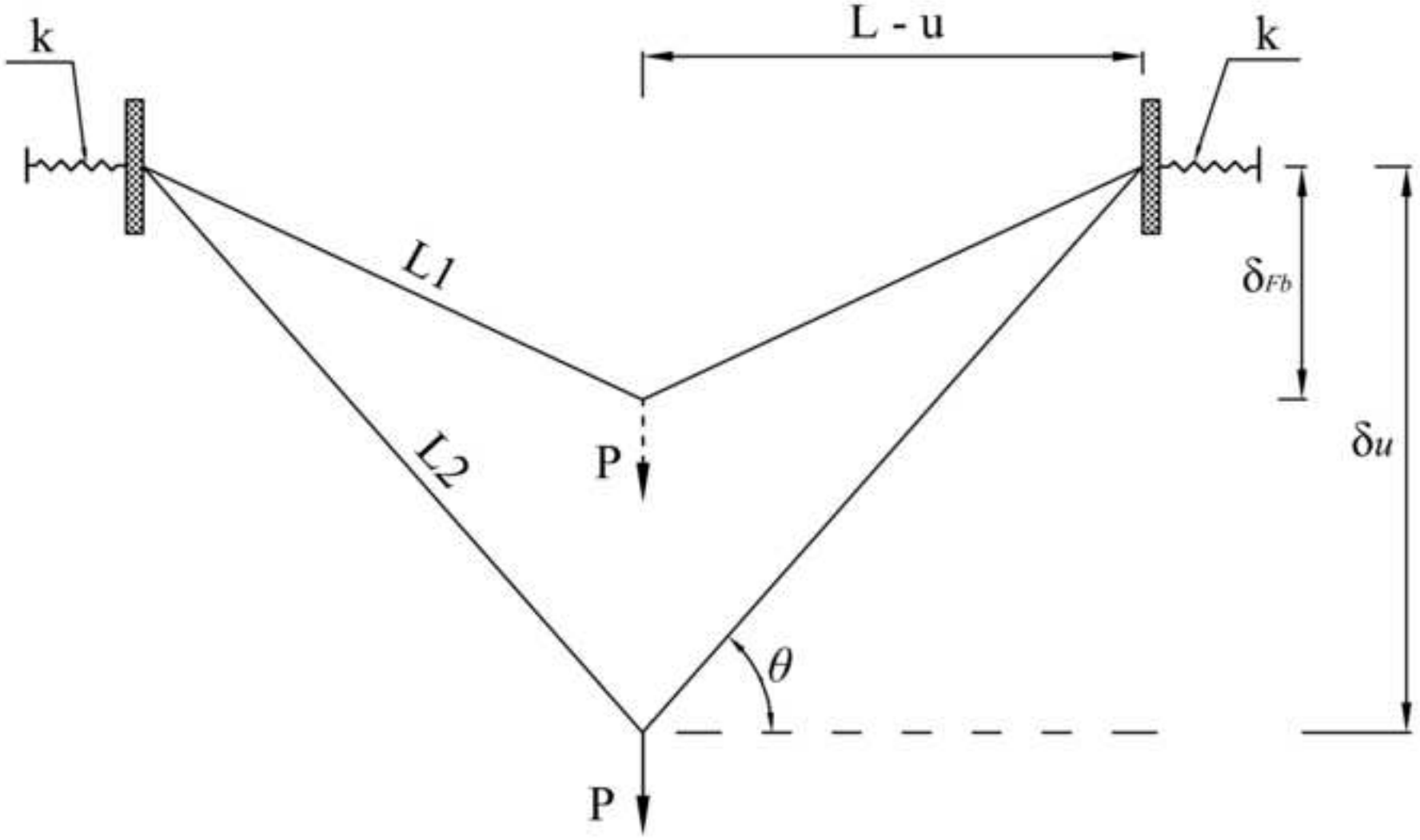

Figure 15

Click here to download Figure 15.tif

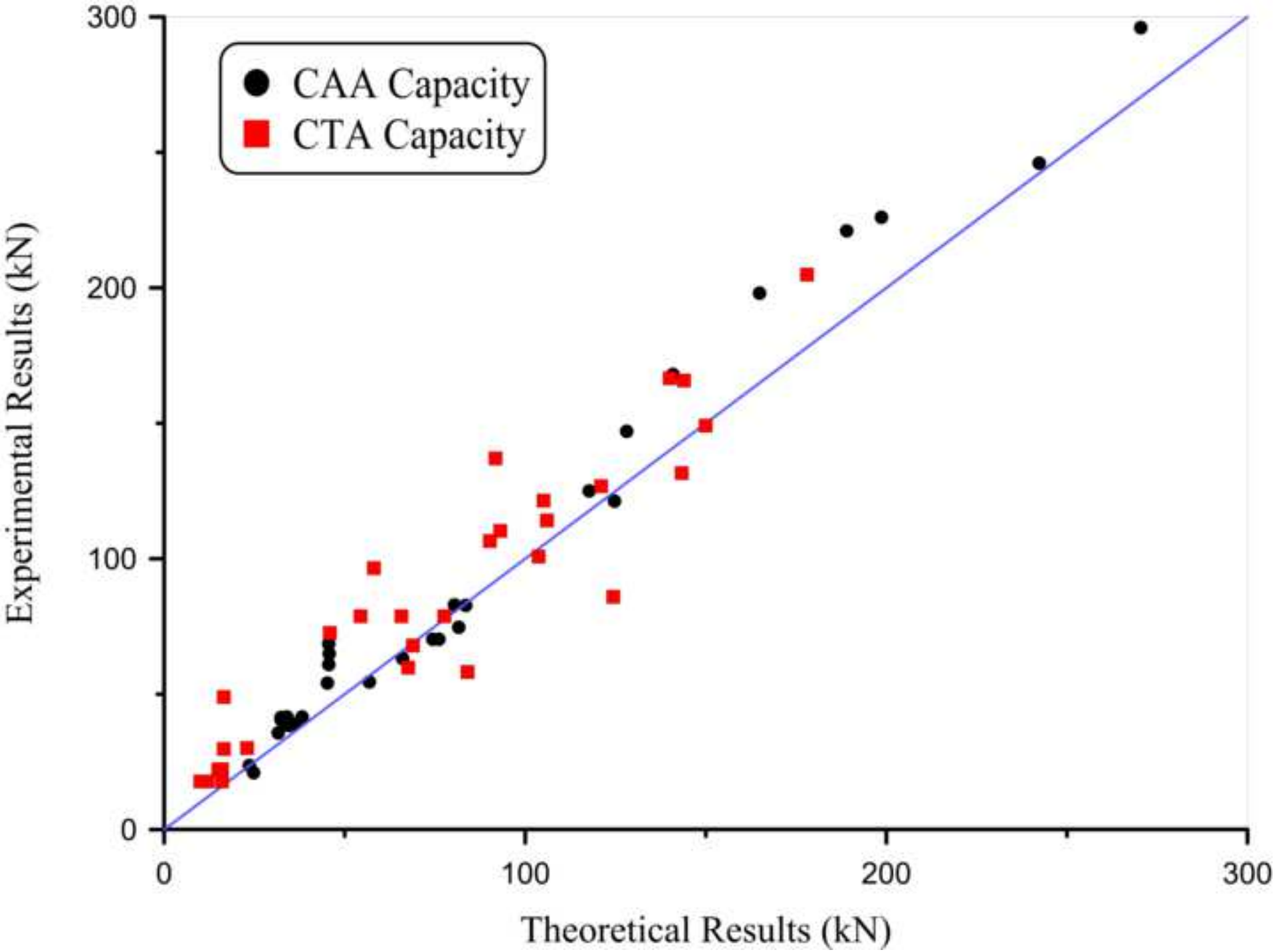

Figure 16

Click here to download Figure 16.tif

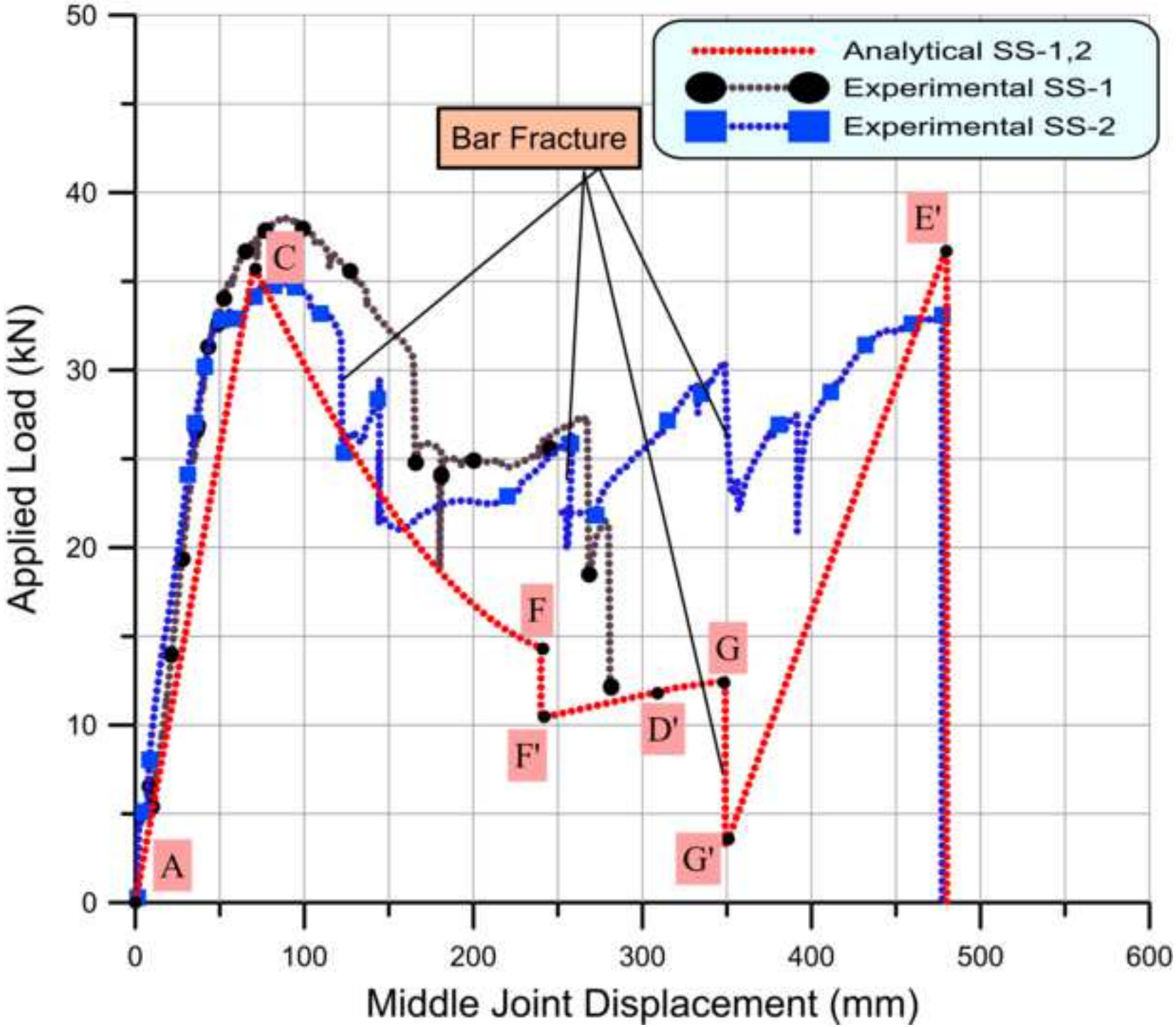

Figure 17

Click here to download Figure 17.tif